



# 1 Decadal trends (2013–2023) in PM<sub>10</sub> sources and oxidative 2 potential at a European urban supersite (Alpine Valley, 3 Grenoble, France)

4 Vy Ngoc Thuy Dinh<sup>1</sup>, Jean-Luc Jaffrezo<sup>1</sup>, Pamela A. Dominutti<sup>1</sup>, Rhabira Elazzouzi<sup>1</sup>, Sophie  
5 Darfeuil<sup>1</sup>, Céline Voiron<sup>1</sup>, Anouk Marsal<sup>1</sup>, Stéphane Socquet<sup>2</sup>, Gladys Mary<sup>2</sup>, Julie Cozic<sup>2</sup>,  
6 Catherine Coulaud<sup>1</sup>, Marc Durif<sup>3,4</sup>, Olivier Favez<sup>3,4</sup>, Gaëlle Uzu<sup>1</sup>

7  
8 <sup>1</sup> Université Grenoble Alpes, CNRS, IRD, INP-G, INRAE, IGE (UMR 5001), 38000 Grenoble, France

9 <sup>2</sup> Atmo Auvergne-Rhône-Alpes (Atmo AuRA), 69500 Bron, France

10 <sup>3</sup> INERIS, Parc Technologique Alata, BP 2, 60550 Verneuil-en-Halatte, France

11 <sup>4</sup> Laboratoire central de surveillance de la qualité de l'air (LCSQA), 60550 Verneuil-en-Halatte, France

12 Correspondence to: Gaëlle Uzu [gaëlle.uzu@univ-grenoble-alpes.fr](mailto:gaëlle.uzu@univ-grenoble-alpes.fr)

## 13 Abstract

14 The identification of particulate matter (PM) sources and the quantification of their contribution to the urban  
15 environment is a necessary input for policymakers to reduce the air pollution impacts. The association between  
16 the PM sources and the oxidative potential (OP) is also a key indicator for evaluating the ability of PM sources to  
17 induce *in-vivo* oxidative stress and lead to adverse health effects, which becomes an emerging metric in the  
18 Directive on ambient air quality (2024/2881/EU). Most studies in Europe have focused on PM and OP sources  
19 in the short term, for only 1 or 2 years. However, the efficiency of reduction policies, trends, and epidemiological  
20 impacts cannot be properly evaluated with such short-term studies due to a lack of statistical robustness. Here,  
21 long-term PM<sub>10</sub> filter sampling at the Grenoble (France) urban background supersite and detailed chemical  
22 analyses were used to investigate decadal trends of the main PM sources and related OP metrics. Positive matrix  
23 factorization (PMF) analyses were conducted on the corresponding 11-year dataset (Jan 2013 to May 2023, n =  
24 1570), enlightening the contributions of 10 PM sources: mineral dust, sulfate-rich, primary traffic, biomass  
25 burning, primary biogenic, nitrate-rich, MSA-rich, aged sea salt, industrial and chloride-rich. The stability of the  
26 chemical profile of these sources was validated by comparison with the profiles retrieved from shorter-term (3  
27 years) successive PMF analyses. A Seasonal-Trend using LOESS decomposition was then applied to evaluate the  
28 trends of these PM<sub>10</sub> sources, which revealed a substantial decrease in PM<sub>10</sub> ( $-0.73 \mu\text{g m}^{-3} \text{yr}^{-1}$ ) as well as that of  
29 many of the PM<sub>10</sub> sources. Specifically, negative trends for primary traffic and biomass burning sources are  
30 detected, with a reduction of 0.30 and  $0.11 \mu\text{g m}^{-3} \text{yr}^{-1}$ , respectively. The OP PM<sub>10</sub> source apportionment in 11  
31 years confirmed the high redox activity of the anthropogenic sources, including biomass burning, industrial, and  
32 primary traffic. Eventually, downward trends were also observed for OP<sub>AA</sub> and OP<sub>DTT</sub>, mainly driven by the  
33 reduction of residential heating and transport emissions, respectively.

34 Keywords: PM<sub>10</sub> source apportionment, OP PM<sub>10</sub> source apportionment, long-term trend, Positive matrix  
35 factorization.



## 36 1. Introduction

37 Particulate matter (PM) is the main atmospheric pollutant that significantly impacts human health, climate, and  
38 the environment (Fuzzi et al., 2015; Grantz et al., 2003; Pope and Dockery, 2006), which is emitted directly or  
39 formed through complex processes in the atmosphere from natural and anthropogenic gaseous precursors. The  
40 identification of PM sources is important to investigate their composition, contribution, and evolution, which is  
41 one necessary input for policymakers to apply strategies in reducing their impact. There are various methodologies  
42 to identify these sources, where receptor models are widely used to perform source apportionment (SA) due to  
43 their flexibility and performance. Positive Matrix factorization (PMF) is one of the most popular among these  
44 receptor models, as it has been developed to allow SA analysis without any prior information other than the  
45 measurement and uncertainty input matrices (Hopke, 2016). Scores of studies using PMF have been applied in  
46 different typologies of sites over the last 15 years, with urban areas being the most common (Hopke et al., 2020;  
47 Viana et al., 2008).

48 The adverse health effects of PM can be assessed through different pathways, one of which uses the concept of  
49 oxidative stress within the lung (Pope and Dockery, 2006). PM has the ability to generate reactive oxygen species  
50 (ROS), which can cause an imbalance with antioxidants in the lungs, eventually causing oxidative stress. This  
51 capacity is evaluated as the oxidative potential (OP) of PM (Ayres et al., 2008; Li et al., 2008; Lodovici and  
52 Bigagli, 2011; Mudway et al., 2020; Nelín et al., 2012; Rao et al., 2018). The redox activity of PM is mainly  
53 dependent on their compositions; nevertheless, the correlation between individual components of PM and OP is  
54 probably not the best approach for understanding the impact of ambient PM because of their complex mixture  
55 preventing the quantification of all components of interest (Borlaza, 2021; Calas et al., 2018; Weber et al., 2018).  
56 Therefore, the relationship between OP and PM sources has been investigated as a more holistic approach (Bates  
57 et al., 2018; Dominutti et al., 2023; Weber et al., 2021). The implementation steps of such an approach can include,  
58 first, a PM source apportionment (SA) (usually using PMF), allowing the identification of PM sources and their  
59 contribution to PM. Then, the relationship between OP and PM sources is investigated by performing some  
60 regression techniques, potentially including linear and non-linear ones (Ngoc Thuy et al., 2024).

61 The OP of PM is becoming an emerging metric for the European regulation on air quality, included in the new  
62 European Air Quality Directive (Directive (EU) 2024/2881) as a recommended measurement at super sites in each  
63 member state in order to improve the knowledge about the variability of the OP and eventually allow the  
64 connections with epidemiological studies. Most previous studies have focused on PM and OP sources over a  
65 relatively short period, typically less than 1 or 2 years (Borlaza et al., 2022; Pietrodangelo et al., 2024; Weber et  
66 al., 2019). Such short-term studies assess the PM and OP sources as well as their contribution, providing  
67 information on the intrinsic OP of PM sources, allowing for the development of OP modeling (Daellenbach et al.,  
68 2020; Vida et al., 2024) and eventually designing some public policies (Borlaza, 2021). However, long-term series  
69 are needed both for evaluating the efficiency of such reduction policies in connection with the evolution of  
70 contributions from sources and also for implementing epidemiological studies (Borlaza-Lacoste et al., 2024).

71 The present study is based on a long-term measurement program conducted in the city of Grenoble (France),  
72 resulting from a sustained collaboration between the local network (Atmo AuRA), the French Reference  
73 Laboratory for Air Quality Monitoring (LCSQA), and the Institute of Environmental Geosciences (IGE) to  
74 investigate long-term evolution of PM<sub>10</sub> sources and OP in the PM<sub>10</sub> as well as their tendencies in the urban  
75 background of the city. Here, we assessed these source contributions from daily ambient PM<sub>10</sub> samples obtained

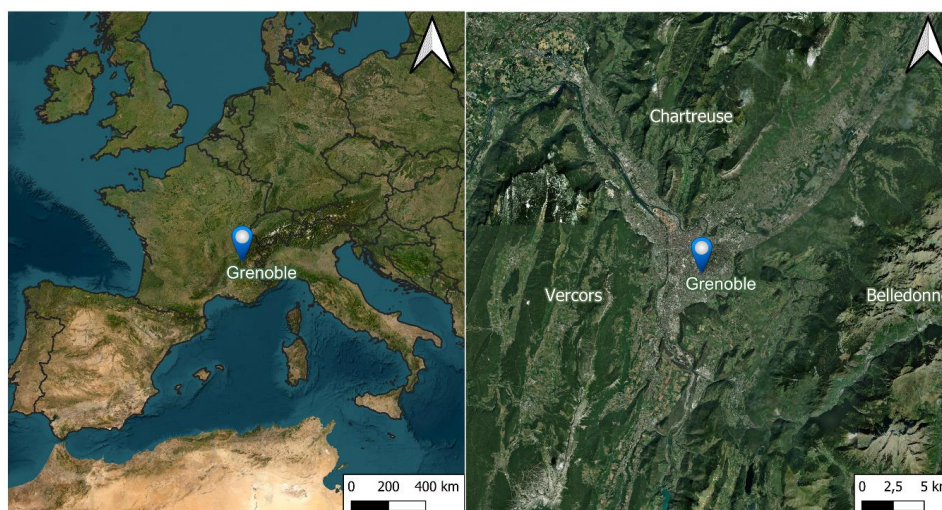


76 from 2013 to 2023 ( $n = 1570$ ) using the EPA PMF model at this site selected as one of the French urban supersites  
77 for the new EU 2024/2881 Air Quality Directive. The database was augmented using imputation techniques in  
78 order to fill some of the gaps in the data, relative to metallic trace elements. Since PMF is rarely applied to such  
79 a long-term database, several evaluations of the validity of solutions were also implemented. The PMF-derived  
80  $PM_{10}$  sources were then used to perform OP SA from 2013 to 2022 ( $n=1570$ ). The trend of  $PM_{10}$  concentration,  
81 of the  $PM_{10}$  sources, and the OP measurements are eventually discussed in relation to several potential factors of  
82 influence.

## 83 **2. Methodology**

### 84 **2.1. Sampling site**

85  $PM_{10}$  daily samples were collected at an urban background site (Grenoble - Les Frênes), in the southern area of  
86 Grenoble, France ( $45^{\circ}09'41''$  N,  $5^{\circ}44'07''$  E). This city is known as the French Alps' capital, sprawling over 18.13  
87  $km^2$  with about 154,000 inhabitants in 2023, but nearly 500,000 within the larger urbanized area (about 15 km  
88 radius). With an average altitude of about 200 masl, the city sits within a complex mountainous geomorphology  
89 and is surrounded by three mountain massifs: Chartreuse, Vercors, and Belledonne (Figure 1). A pendular wind  
90 regime between the three valleys of the basin regulates the ventilation of the atmosphere, with frequent thermal  
91 inversion during cold periods, leading to the accumulation of pollutants. The air quality is monitored at several  
92 sites in Grenoble by the regional agency (Atmo AuRA), including the urban background site of this study, which  
93 is equipped with a large array of instruments. Particularly, the chemistry of  $PM_{10}$  collected on filters has been  
94 speciated at this site since 2008, within several programs, including the CARA program from the French Ministry  
95 of Environment (Favez et al., 2021) and several research programs such as QAMECS (Borlaza et al., 2021), or  
96 SOURCES (Weber et al., 2019). Many aspects of air quality in Grenoble were reported for this site, including the  
97 characteristics of secondary anthropogenic PM fraction (Baduel et al., 2009, 2012; Favez et al., 2010; Tomaz et  
98 al., 2016, 2017), of the biogenic PM components (Brighty et al., 2022; Samaké et al., 2019a, a), as well as the PM  
99 OP (Borlaza, 2021; Dominutti et al., 2023; Weber et al., 2021). Several studies of one-year PM sources  
100 apportionment were also performed in 2013 (Srivastava et al., 2018) and 2017-2018 (Borlaza et al., 2021). Despite  
101 the difference in input data and periods of the studies, similar main sources of PM were quantified in both studies,  
102 including residential heating, traffic, and secondary inorganic aerosol (SIA).



103  
104  
105 **Figure 1.** The sampling site is located in the Southeast of France (left figure), surrounded by 3 mountains massifs (Vercors, Chartreuse, and Belledonne). Background map: ESRI satellites.

## 106 2.2. Sampling and chemical analyses

### 107 2.2.1. PM<sub>10</sub> and their inorganic and organic composition

108 The daily PM<sub>10</sub> sampling was performed every third day from 02/01/2013 to 28/05/2023, on 150 mm-diameter  
109 quartz fibre filter (Tissu-quartz PALL QAT-UP 2500 diameter 150 mm) using high-volume samplers (Digital  
110 DA80, 30 m<sup>3</sup> h<sup>-1</sup>). A weekly PM<sub>10</sub> sampling was conducted during the same period using a low-volume sampler  
111 (Partisol, 1 m<sup>3</sup> h<sup>-1</sup>) onto 47mm diameter quartz fibre filters (Tissuquartz PALL QAT-UP 2500 diameter 47 mm).  
112 The processes of preparation, handling, and storing filters, in order to guarantee optimum quality for chemical  
113 analyses were presented in Borlaza et al. (2021). Field blank filters were also collected (about 8-10% of the total  
114 samples) to estimate the detection limits and evaluate the filter contamination during the overall handling and  
115 analysis processes.

116 The daily PM<sub>10</sub> samples (n = 1570) and field blanks were analyzed for elemental carbon (EC) and organic carbon  
117 (OC), major ions (Cl<sup>-</sup>, NO<sub>3</sub><sup>-</sup>, SO<sub>4</sub><sup>2-</sup>, Na<sup>+</sup>, NH<sub>4</sub><sup>+</sup>, K<sup>+</sup>, Mg<sup>2+</sup>, Ca<sup>2+</sup>), methanesulfonic acid (MSA), anhydrous sugar  
118 and saccharides (levoglucosan, mannosan, arabitol, mannitol), and trace elements (As, Ba, Cd, Cr, Cu, Mn, Ni, Pb,  
119 Sb, V, Zn). However, the concentrations of the daily trace elements were analyzed only in 3 periods, including:  
120 (1) from January 2nd, 2013 to December 31st, 2013 (n = 122), (2) from February 28th, 2017 to March 13th, 2018  
121 (n = 125), (3) from June 30th, 2020 to June 18th, 2021 (n=115). The weekly samples and blanks were analyzed  
122 for trace metal concentrations for the whole sampling period (n = 842).

123 All analyses were previously described in detail (Borlaza et al., 2021). In brief, EC and OC analysis was performed  
124 using a Sunset Lab analyser with the EUSAAR2 thermo-optical protocol. The eight major ionic components and  
125 MSA were analyzed, after aqueous extraction of the filters using orbital shaking, by ionic chromatography using  
126 an ICS3000 dual-channel chromatograph (Thermo-Fisher) with a CS16 column for cation analysis and an AS11  
127 HC column for anion analysis. The anhydrous-sugar and saccharides analyses were performed on the same water  
128 extract by an HPLC method using PAD (Pulsed Amperometric Detection) (model Dionex DX500 + ED40) with  
129 Metrosep columns (Carb 1-Guard+A Supp15-150+Carb1-150) in the period before the year 2017. From 2017 to



the present, the measurement with ICS 5000 with pulsed amperometric detection (HPLC-PAD) was performed following the CEN method (European committee for standardization, 2024). The analysis is isocratic with 15% eluent of sodium hydroxide (200 mM), sodium acetate (4 mM), and 85% water at 1 mL min<sup>-1</sup>. The daily and weekly metals were measured by Inductively coupled plasma mass spectroscopy (ICP-MS) (ELAN 6100 DRC II PerkinElmer or NEXION PerkinElmer). The measurement was performed on the mineralization of a 38 mm diameter punch of each filter, using 5 mL of HNO<sub>3</sub> (70 %) and 1.25 mL of H<sub>2</sub>O<sub>2</sub> for 30 min at 180°C in a microwave.

### 2.2.2. OP analysis

Two complementary OP assays, including the two probes ascorbic acid (AA) and dithiothreitol (DTT) were performed on the same filters with PM<sub>10</sub> components analysis (from 02/01/2013 to 28/05/2023, n = 1570). Filter samples are extracted using a simulated lung fluid during 1h15 at 37°C, pH 7.4, as described in Calas et al. (2017), which creates a physiological environment for the extraction. The AA method quantifies the consumption of ascorbic acid, an endogenous antioxidant in the lung, by PM and was described in Calas et al. (2017, 2018). The reaction mixture (extract + AA) was transferred to UV-transparent 96-well plates (CELLSTAR, Greiner-Bio), and the residual AA was measured at 265 nm with a TECAN Infinite M200 Pro spectrophotometer. The AA consumption rate (nmol min<sup>-1</sup>) reflects the capacity of PM<sub>10</sub> to catalyze electron transfer from AA to molecular oxygen.

DTT assay relies on dithiothreitol, a chemical surrogate for cellular reducing agents, allowing for emulation of in vivo interaction among PM<sub>10</sub> and biological reducing agents (for example, nicotinamide adenine dinucleotide (NADH), nicotinamide adenine dinucleotide phosphate oxidase (NADPH)). After incubation of the PM suspension within the lining fluid with DTT, the remaining DTT was titrated with 5,5'-dithiobis-(2-nitrobenzoic acid) (DTNB) to form 5-mercapto-2-nitrobenzoic acid (TNB). Absorbance at 412 nm (TECAN Infinite M200 Pro) in 96-well plates provided the concentration of unconsumed DTT, from which the DTT consumption rate (nmol min<sup>-1</sup>) was calculated. The batches were standardized using common external references to ensure consistency between batches.

After analysis, the OP activities were blank subtracted and then normalized using the PM<sub>10</sub> mass concentration and the sampling air volumes. The mass-normalized OP (OP<sup>m</sup>, nmol min<sup>-1</sup> μg<sup>-1</sup>) represents the intrinsic OP of 1 μg PM, while the volume-normalized OP (OP<sup>v</sup>, nmol min<sup>-1</sup> m<sup>-3</sup>) represents PM-derived OP per m<sup>3</sup> of air. Each sample is analyzed in triplicate for AA and triplicate for DTT, respectively. Consequently, the OP values presented in the study are the mean and the standard deviation of these replicates.

### 2.2.3. Vertical temperature and other ancillary measurements

Vertical temperature and humidity were measured every 30 minutes from November 2017 to May 2023 using Tinytag TGP-4500 from Gemini Data Loggers. A Stevenson Type Screen protects each Tinytag loggers from radiant heat (direct sunlight). Sensors are installed at a minimum of 3m from the ground. The measurements have been performed at different elevations of the Bastille hill, located a few hundred meters from the city center (5°43'37.0" E, 45°11'40.8" N), including z = 230, 309, 496, 916m altitudes.

Further, measurement of the PM<sub>10</sub> mass was conducted (hourly) using tapered element oscillating microbalances equipped with filter dynamics measurement systems (TEOM-FDMS) at the same site as the filter collection. The



PM concentration used in this study is the 24-hour average concentration, which is associated with the days of filter-based sample measurement (from 02/01/2013 to 28/05/2023).

170

### 2.3. Multivariate imputation by chained equations (MICE)

The daily concentration of metals was only accessed in some periods, with the number of samples being 362 of the total of 1570 samples, which would severely limit the size of the inputs for the PMF processing. We used the weekly concentration measured over the whole period to estimate the missing daily data using an imputation method. The daily concentration of metals was imputed by using the MICE algorithm implemented with multilinear regression (Azur et al., 2011). These values were modeled conditionally depending on the observed values of the daily PM<sub>10</sub> and PM<sub>10</sub> components concentration (i.e., weekly concentration, PM<sub>10</sub>, and PM<sub>10</sub> components concentration). These components are OC, EC, MSA, Levoglucosan, Mannosan, Polyols, NO<sub>3</sub><sup>-</sup>, SO<sub>4</sub><sup>2-</sup>, Na<sup>+</sup>, NH<sub>4</sub><sup>+</sup>, K<sup>+</sup>, Mg<sup>2+</sup>, Cl<sup>-</sup>, Ca<sup>2+</sup>. The data preparation and imputation processes are implemented through 4 main steps, as presented in S1 and Figure S1, Supplement. The validation of this imputation is shown in Table S1 and Figure S2.

### 2.4. Persistent inversions detection

Thermal inversion occurs when the vertical temperature gradient between the ground-based and higher-altitude stations is positive. However, this constraint is restrictive and limits thermal inversion detection, especially when the calculation is on average daily temperature (Largeron and Staquet, 2016). Hence, the persistent inversion is detected, as discussed in Largeron and Staquet (2016), for days with :

$$average \left( \frac{T_{916} - T_{230}}{\Delta z} \right)_{Daily} > Mean \left( \frac{T_{916} - T_{230}}{\Delta z} \right)_{Winter} \quad (1)$$

for more than 72 consecutive hours

with:

$T_{916} - T_{230}$  is the difference between temperature at ground-base station ( $z = 230\text{m}$  altitude) and at high-elevation station ( $z = 916\text{m}$ );

$\Delta z$  is the difference between the height of high and low elevations;

$\frac{T_{916} - T_{230}}{\Delta z}$  : is the bulk temperature gradient between  $z = 230$  and  $z = 916\text{m}$ ;

$Mean \left( \frac{T_{916} - T_{230}}{\Delta z} \right)_{Winter}$  : is the mean bulk temperature gradient in wintertime (from November to March).

### 2.5. Positive Matrix Factorisation (PMF)

#### 2.5.1. PMF input

EPA PMF 5.0 (Gary Norris et al., 2014) was used to identify and quantify the PM<sub>10</sub> sources based on the observed concentrations and their related uncertainties. The concept of PMF is to use the weighted least square fit method and apply a non-negative constraint with the weight calculated based on analysis uncertainties (Paatero and Tappert, 1994) (Eq. (S1), Supplement S2). In this study, the input matrix of the PMF comprises 25 chemical species, including PM<sub>10</sub> (set as the total variable), carbonaceous fractions (OC\*, EC), ions (Cl<sup>-</sup>, NO<sub>3</sub><sup>-</sup>, SO<sub>4</sub><sup>2-</sup>, Na<sup>+</sup>, NH<sub>4</sub><sup>+</sup>, K<sup>+</sup>, Mg<sup>2+</sup>, Ca<sup>2+</sup>), organic tracers (MSA, levoglucosan, mannosan, polyols) and trace metals (As, Ba, Cd, Cr, Cu, Ni, Pb, Sb, V, Zn). The trace metals were the daily measured metals in some periods (2013, 2017-2018,





204 2020-2021) and the daily imputed metals. The OC\* (=OC minus the sum of the carbon mass from the organic  
205 tracers used in the input variables) was used to avoid considering twice the mass of C atoms in organic markers.  
206 Polyols were calculated as the sum of arabitol and mannitol, supposing that their origin is similar (Samaké et al.,  
207 2019a). The input uncertainties were calculated based on the concentrations and the uncertainties in the analysis  
208 (Gianini et al., 2012; Waked et al., 2014). Details on the calculation of OC\* and uncertainties of PMF input are  
209 presented in Section S3, Supplement. The selection of the input variables is guided by our previous yearly PMF  
210 studies at this site (Borlaza et al., 2021; Srivastava et al., 2018; Weber et al., 2019).

### 211 2.5.2. Set of constraints

212 The application of PMF constraints is recommended in the European guide on air pollution source apportionment  
213 with receptor models (Belis et al., 2014) to avoid mixing between some factors and reduce the uncertainty of the  
214 rotational ambiguity. The constraints used in this study are also based on the previous PMF studies in Grenoble  
215 (Borlaza et al., 2021; Srivastava et al., 2018; Weber et al., 2019) and are detailed in Table S3.

### 216 2.5.3. Choice of the final PMF solution

217 Several solutions, including those from 4 to 11 factors, were investigated to determine the optimal output. This  
218 selection is based on the ratio of  $Q_{\text{true}}/Q_{\text{robust}}$  (evaluating the outlier's effect), the clarity of the chemical profile,  
219 the contribution of factors to  $\text{PM}_{10}$ , the correlation between measured and predicted concentration, and the stability  
220 of the solution. This stability was evaluated using the bootstrapping (BS) and displacement (DISP) methods. BS  
221 analysis randomly resamples the data observation matrix and uses it to run a new PMF. The base-run and boot-  
222 run factors are matched if their correlation exceeds the threshold (generally chosen at 0.6). DISP estimates each  
223 species' uncertainty in the factor profile by fitting the model many times until this variable turns displaced (upper  
224 or lower) from its fitted value. The details of the set criteria for validation are presented in S4.

225 To evaluate the stability of the PMF solution over time (including possible changes in the chemical profiles of the  
226 sources), we also implemented separated PMF SA for every successive period of 3 years (2013-2016, 2017-2020,  
227 2021-2023) and then we investigated the homogeneity of the chemical profiles by using the Pearson distance (PD)  
228 and standardized identity distance (SID) metrics (Belis et al., 2015). The chemical profiles of PMF solutions every  
229 3 years and 11 years, and those published in Borlaza et al. (2021) are compared to assess the homogeneity of the  
230 chemical profiles.

## 231 2.6. Regression techniques for $\text{PM}_{10}$ OP SA

232 The regression technique is applied to apportion  $\text{OP}^v$  (AA, DTT) and PMF-derived  $\text{PM}_{10}$  sources' contribution, as  
233 expressed in Eq.2. Principally,  $\text{OP}^v$  ( $\text{nmol min}^{-1} \text{m}^{-3}$ ) is treated as a dependent variable, and PMF-derived  $\text{PM}_{10}$   
234 sources' contribution ( $\mu\text{g m}^{-3}$ ) are independent variables. The OP SA methodology in this study follows the  
235 methodology reported by Ngoc Thuy et al. (2024).

$$236 \quad \text{OP}_v = \sum_p^{i=1} \text{OP}_m^i * \text{PM}^i + e \quad (2)$$

237 Where:

238  $\text{OP}_v$  is the volume-normalized OP ( $\text{nmol min}^{-1} \text{m}^{-3}$ )

239  $p$  is the number of PMF-derived  $\text{PM}_{10}$  sources



240  $OP_m^i$  is the regression slope, denoted as the intrinsic OP of source  $i$  ( $\text{nmol min}^{-1} \mu\text{g}^{-1}$ )

241  $PM^i$  is the contribution of source  $i$  to  $PM_{10}$  ( $\mu\text{g m}^{-3}$ )

242  $e$  is the residual of the regression technique ( $\text{nmol min}^{-1} \text{m}^{-3}$ )

243 The appropriate regression tool is selected based on the collinearity among independent variables and the variance  
244 of regression residuals (Ngoc Thuy et al., 2024). The collinearity among PMF-derived sources was tested using  
245 the variance inflation factor (VIF), which is calculated using Eq. (S3) in Supplement S2 (Craney and Surles, 2002;  
246 O'Brien, 2007; Rosenblad, 2011). The variance of the regression residual is assessed using the Goldfeld-Quandt  
247 test (Goldfeld and Quandt, 1965) to investigate if the regression residual varies by the value of the dependent  
248 variable (OP<sup>n</sup>). The most appropriate regression method is selected among a wide choice of possible tools  
249 (including ordinary least square, weighted least square, positive least square, Ridge, Lasso, random forest, and  
250 multiple layer perceptron), following the methodology developed by Ngoc Thuy et al. (2024). It is performed with  
251 considering the characteristics of the data and comparing the accuracy metrics (R-square, root mean square error,  
252 and mean absolute error) for each of them. For instance, if the regression residual is constant (homoscedasticity),  
253 the model ordinary least square (OLS) and Positive least square (PLS) are satisfactory. On the other hand, if the  
254 regression residual varied with the dependent variable (heteroscedasticity), the models incorporating some sort of  
255 weighting are chosen (including weighted least squares (WLS) and weighted positive least squares (wPLS)),  
256 where the weighting is the standard deviation of replicated OP analyses.

257 The most appropriate model was trained by randomly choosing 80% of the dataset and validated with the  
258 remaining 20%. The model was run 500 times to ensure the robustness of the results, especially considering the  
259 remarkable seasonality of many components in the dataset. The contribution to OP of each source is calculated  
260 by multiplying its contribution to  $PM_{10}$  with the arithmetic mean intrinsic OP (or regression slope) of the 500  
261 iterations.

## 262 **2.7. Seasonal-trend using LOESS decomposition**

263 Seasonal-trend decomposition using LOESS (SLT) was developed by RB Cleveland et al. (1990) and is a robust  
264 method for decomposing time series into trends, seasonality, and residuals. This method uses LOESS, a method  
265 for estimating the non-linear relationships to decompose a time series. In our case, we used monthly average  
266 concentration as input data in order to have a more robust data set, smoothing high variability noise. The trend  
267 component is first calculated by applying a convolution filter to the data. Then, this trend is removed from the  
268 series. Finally, the average of this detrended in each period is the seasonal component. The residuals can be  
269 explained neither by trend nor by season. The STL is an iterative model that uses LOESS to smooth seasonal and  
270 trend components to obtain the minimum residuals. Further, in STL decomposition, the outliers in the data are  
271 given less weight in the estimation of trend and season. The STL model is described in the equation below:

$$272 \quad y_t = S_t + T_t + R_t \quad (t = 1, 2, \dots, n) \quad (3)$$

273 where, in our case,  $y_t$  is the monthly contribution of PMF-derived sources,  $S_t$  is the seasonal component,  $T_t$  is the  
274 trend component, and  $R_t$  denotes the residual component. The seasonal frequency was chosen 6 months before  
275 and 6 months after the evaluated month (seasonal frequency = 13 months) to estimate the yearly trend cycle.  
276 Hence, the first and last 6 months of the decomposition time series were removed from the results to prevent edge  
277 effects.





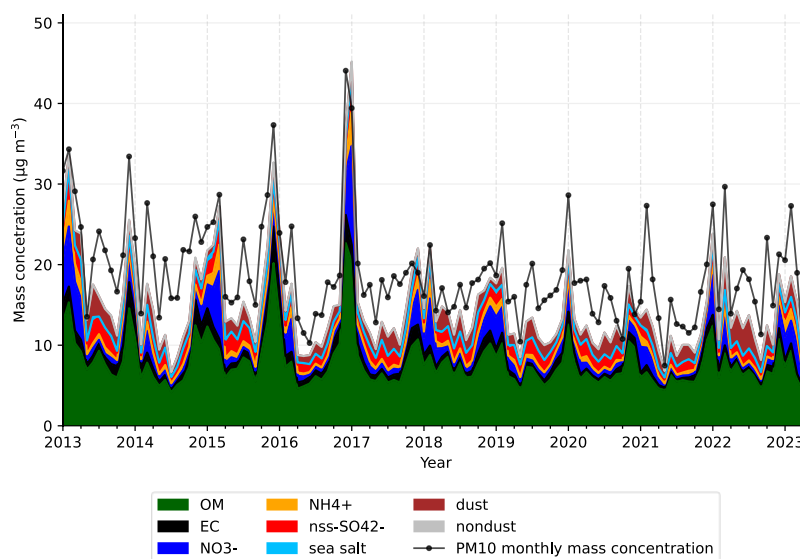
278 The long-term trend of PM<sub>10</sub> sources was accessed by applying the STL model to the monthly contribution of  
279 sources to PM<sub>10</sub> (output of PMF). The fit line of the trend was assessed by using ordinary least squares linear  
280 (OLS). The annual rate change of the trend is the slope of the fit line multiplied by 12 months ( $\mu\text{g m}^{-3} \text{ yr}^{-1} / \text{nmol}$   
281  $\text{min}^{-1} \mu\text{g}^{-1} \text{ yr}^{-1}$ ). The STL decomposition and the fit line of the trend were performed in Python 3.9 using the  
282 package "statsmodels" (Seabold and Perktold, 2010).

### 283 3. Results and discussion

#### 284 3.1. Evolution of PM<sub>10</sub> concentration and chemical components

285 The annual average concentration of PM<sub>10</sub>, considering all available daily measurements, is  $19.0 \pm 10.6 \mu\text{g m}^{-3}$  for  
286 the whole studied period (2013-2023). The highest annual concentration is observed in 2013 ( $24.4 \pm 13.7 \mu\text{g m}^{-3}$ ),  
287 and the lowest is in 2021 ( $15.3 \pm 9.8 \mu\text{g m}^{-3}$ ). The number of days with concentrations surpassing the European  
288 standard daily thresholds ( $40 \mu\text{g m}^{-3}$ ) is 176 days in 11 years, representing 4.6% of the total observed days, which  
289 are principally found in the cold season (Nov, Dec, Jan, Feb, Mar).

290 The PM<sub>10</sub> main components are organic matter (assuming  $\text{OM} = 1.8 * \text{OC}$  (Favez et al., 2010)), representing on  
291 average over the overall period  $41.3 \pm 8.0\%$  of PM<sub>10</sub> mass concentration, followed by dust ( $9.6 \pm 4.4\%$ ), nitrate  
292 ( $\text{NO}_3^-$ ,  $7.5 \pm 6.2\%$ ), non-sea salt sulfate ( $\text{nss-SO}_4^{2-}$ ,  $7.4 \pm 2.4\%$ ), elemental carbon (EC,  $5.5 \pm 2.5\%$ ), ammonium  
293 ( $\text{NH}_4^+$ ,  $3.9 \pm 2.0\%$ ), sea salt ( $\text{Na}^+$  and  $\text{Cl}^-$ ,  $1.7 \pm 0.8\%$ ) and other non-dust elements (Cu, Pb, V, Zn, representing  
294  $0.2 \pm 0.1\%$ ). These main composition fractions are estimated using the formula as shown in S2, Eq. (S4). The  
295 monthly evolutions of PM<sub>10</sub> and its main chemical components for the whole period are shown in Figure 2. The  
296 maximum concentration of PM<sub>10</sub> was observed in winter months (December, January, and February),  
297 corresponding to the highest concentration of OM and EC ( $7.82 \pm 3.11 \mu\text{g m}^{-3}$  and  $1.09 \pm 0.74 \mu\text{g m}^{-3}$ , respectively).  
298 Nitrate concentrations are higher in the middle of winter and the early spring, corresponding also with the high  
299 concentrations of ammonium ( $1.63 \pm 1.87$  and  $0.78 \pm 0.62 \mu\text{g m}^{-3}$ ). The agricultural activities (especially manure  
300 spreading) could explain this high contribution in spring under humidity and temperature conditions favoring the  
301 condensation of ammonium nitrate in the particulate phase. Nss-sulfate concentrations are more abundant in the  
302 warmer season (summer), where the photochemical production is favorable. No clear seasonal pattern could be  
303 observed for other components (sea salt, dust, non-dust, estimated as described in section S2), suggesting that the  
304 emissions of these components are stable for the whole year. At first glance, decreasing trends appear visible for  
305 PM<sub>10</sub> and OM, EC,  $\text{NO}_3^-$ ,  $\text{NH}_4^+$ , and non-dust components, while sea salt, dust, and  $\text{nss-SO}_4^{2-}$  do not seem to  
306 present significant trends. With chemical components coming from several emission sources, an advanced  
307 analysis, including a PMF model followed by an STL decomposition, was performed to assess the trend of PM<sub>10</sub>  
308 sources. The result of the PMF model is presented in section 3.2, and the tendencies of PM<sub>10</sub> sources and OP are  
309 shown in sections 3.3 and 3.4, respectively.



310  
311  
312

**Figure 2. The average monthly evolution of PM<sub>10</sub> and its main components from 2013 to 2023. The line represents the monthly average concentration of PM<sub>10</sub> measured by TEOM-FDMS.**

313

### 3.2. PM<sub>10</sub> sources apportionment

314

#### 3.2.1. PMF chemical profiles

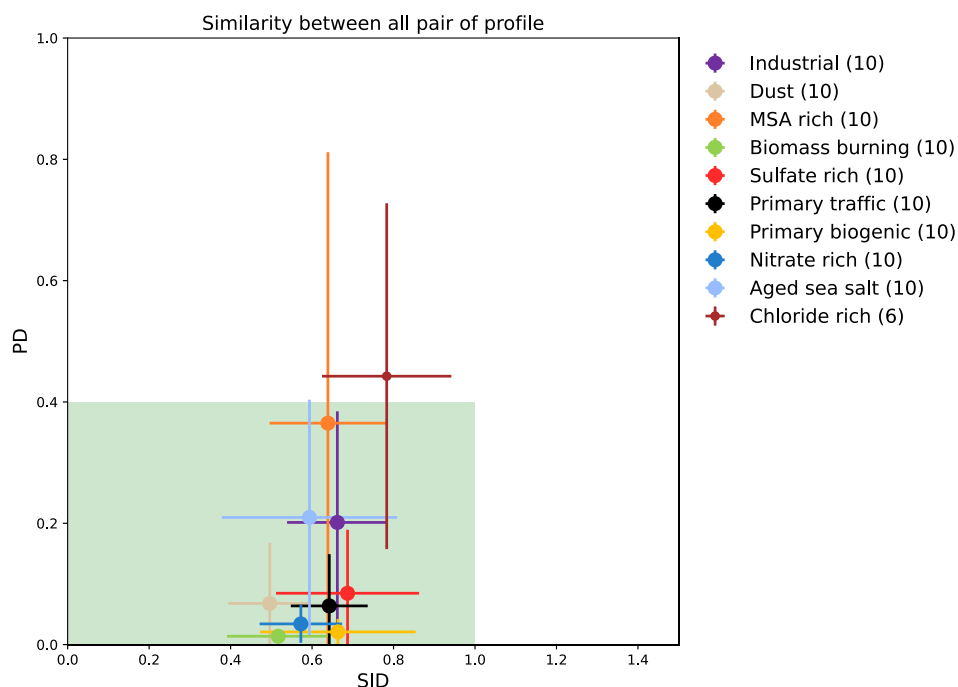
315 Using a unique chemical profile for each of the sources for such a long-term period can potentially limit the  
316 assessment of its evolution (Borlaza et al., 2022). To evaluate such a phenomenon in our case, we investigated  
317 the chemical profile and contribution of PM<sub>10</sub> sources for three distinct periods (2013-2016, 2017-2021, 2022-  
318 2023) and compared the results with those for the full 11-year period, as well as to the results presented in (Borlaza  
319 et al. (2021) for the year 2017. Particularly, we checked the similarity of the chemical profiles of these PMF  
320 solutions using PD and SID metrics (Belis et al., 2015).

321 For each SA, the PMF solution was tested from 4 to 11 factors and validated by the criteria presented in section  
322 S4. The results of these validations ( $Q_{\text{true}}/Q_{\text{robust}}$ , bootstrap run, displacement run, and statistical validation) are  
323 presented in S5, Tables S4, S5 and S6. The runs of 4 to 9 factors returned at least one merging factor, and the  
324 solution with 11 factors led to a factor without geochemical identity. Finally, for each PMF tested (11 years, 2013-  
325 2016, 2017-2021, 2022-2023), the best solution includes 10 PM<sub>10</sub> sources, with mineral dust, sulfate-rich, primary  
326 traffic, biomass burning, primary biogenic, nitrate-rich, MSA-rich, aged sea salt, industrial, and chloride-rich.

327 The similarity of the chemical profiles is presented in Figure 3. Most of the factors (i.e., aged sea salt, mineral  
328 dust, primary biogenic, biomass burning, primary traffic, industrial, nitrate-rich, and sulfate-rich) present quite  
329 homogenous chemical profiles over the 3 successive periods, indicating that these source profiles are quite stable  
330 during the full 11-year period and similar compared to sources reported in Borlaza et al. (2021). The MSA-rich  
331 and chloride-rich sources are the most divergent but are still within the limit of the accepted PD and SID range;  
332 however, their standard deviations for PD are slightly higher than for the other sources (Figure 3). This is due to  
333 differences in the contributions of  $\text{SO}_4^{2-}$  in the chemical profile of MSA-rich, which varied from 6 % to 17%, and  
334 that of  $\text{Cl}^-$  (73% - 83%) in the chloride-rich factor. In a previous study, Weber et al. (2019) also reported that the



335 proportion of  $\text{SO}_4^{2-}$  in the MSA-rich source can significantly vary across French sites, from 6% to 24%. The  
 336 chloride-rich source in our study (previously named sea/road salt in Borlaza et al. (2021)) is essentially composed  
 337 of a high proportion of  $\text{Cl}^-$ , with less than 10% of  $\text{Na}^+$  and some metals (Cu, Mn, Ni, V). This source is detected  
 338 in other alpine valley environments (Glojek et al., 2024), with a similar temporal evolution as here. Since chloride  
 339 depletion from the particulate phase can greatly depend on solar radiation, relative humidity, and temperature, the  
 340 chemical profile of this factor can vary on different time scales. This source was also observed to be heterogeneous  
 341 in the three neighboring sites investigated within 15 km in the previous study in Grenoble (Borlaza et al., 2021).  
 342 Nevertheless, it should be noted that it represents only a very minor fraction of the  $\text{PM}_{10}$  total mass (about 1%).  
 343 With these stabilities of the chemical profiles over the years, the solution for the 11-year SA is considered suitable  
 344 for further data analyses in this paper. In the next section (3.3.2), we investigate how the contribution of these  
 345 sources to total  $\text{PM}_{10}$  loadings changed over time.



346 **Figure 3. Similarity plots of the chemical profiles of the solution for the 11-year SA against the 3 SA solutions every 3**  
 347 **years, and those presented by Borlaza et al. (2021). The shaded area (in green) shows the limit of the homogeneous**  
 348 **chemical profile. For each point, the error bars represent the standard deviation when comparing all pairs of SA**  
 349 **solutions (number of pairs in parentheses in the legend).**  
 350

### 351 3.2.2. Variations of the source's contribution in the 11-year PMF SA

352 As presented in Figure 4, the optimal PMF solution for the 11-year time series identifies 10  $\text{PM}_{10}$  sources, with  
 353 the contributions of mineral dust (20.9%), sulfate-rich (19.7%), traffic (16.0%), biomass burning (13.5%), primary  
 354 biogenic (10.7%), nitrate-rich (7.2%), MSA-rich (6.2%), industrial (2.2%), aged sea salt (2.5 %), and chloride-  
 355 rich (1.0%). The chemical profile and contribution of each source are shown in Figures S3 and S4, respectively.  
 356 Even though the chemical profiles are homogenous, the contributions of these sources show minor differences  
 357 from those reported for this same site by Borlaza et al. (2021) and Srivastava et al. (2018), partly because of the



358 differences in the respective periods of the studies. However, the main sources are similar, i.e., SIA (nitrate and  
359 sulfate-rich), mineral dust, biomass burning, and primary traffic. Similar general results are also presented for  
360 Swiss Alpine (Ducret-stich and Tsai, 2013), French Alpine (Weber et al., 2018), and Slovenian Alpine areas  
361 (Glojek et al., 2024), showing biomass burning and secondary inorganic aerosols being the most abundant  
362 contributions to PM mass. Primary biogenic and MSA-rich sources are the biogenic sources rarely reported in the  
363 literature; however, they account together for 17% of total PM<sub>10</sub> mass on average in our study, which is in line  
364 with those reported in urban background sites in France (Samaké et al., 2019b; Weber et al., 2019). The absolute  
365 PM<sub>10</sub> source contributions are also compared to the average annual concentration of PM<sub>10</sub> mass to demonstrate  
366 the ability of the PMF model to reconstruct the PM<sub>10</sub> mass. The difference between observed and reconstructed  
367 PM<sub>10</sub> concentrations on the 11-year average is about 1 µg m<sup>-3</sup> (5 %), with no more than 2 µg m<sup>-3</sup> for any single  
368 year, demonstrating that the PMF model performs well at reconstructing the PM<sub>10</sub> concentrations.

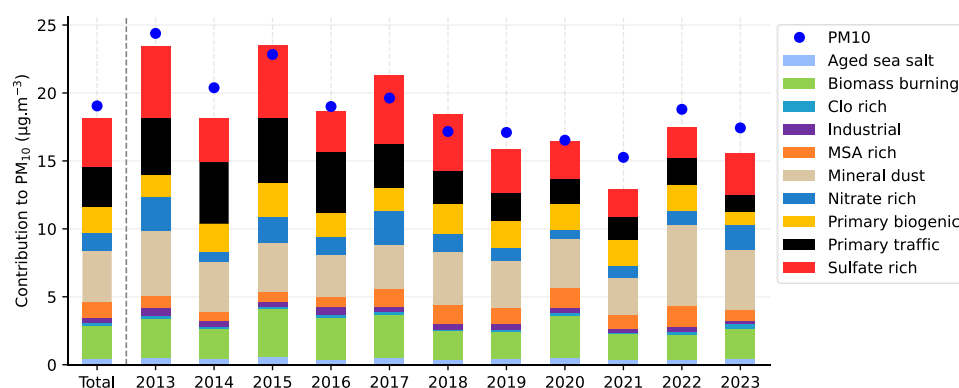


**Figure 4. The absolute average contribution of sources to PM<sub>10</sub> for every year and the 11 years (total), and the concentration of PM<sub>10</sub> (blue circle).**

372 Significant trends in source contributions over this 11-year period are detected (and discussed in section 3.3);  
373 nevertheless, the main contributors to the total PM<sub>10</sub> mass do not change, with mineral dust, biomass burning,  
374 sulphate-rich, nitrate-rich, and primary traffic being the main contributors to PM<sub>10</sub>. The highest PM<sub>10</sub>  
375 concentrations (observed in winter/spring 2013 and 2015) are associated with the highest contribution of SIA and  
376 biomass burning sources. On the other hand, the relative contribution of SIA and biomass burning showed a  
377 negligible difference (varied from 0.3 to 4%) between these years compared to 2014 and 2016 (Figure S5). The  
378 lowest PM<sub>10</sub> annual concentration was detected in 2021, notably when the third COVID-19 pandemic lockdown  
379 restrictions applied in France. In addition, the relative contributions (see Figure S5) showed only small changes  
380 compared to those in other years, with an increasing contribution of primary biogenic sources in 2021 (4%  
381 compared to 2020), and only a very light decrease in the anthropogenic sources.

382 The decrease in PM<sub>10</sub> annual average concentrations observed since 2017 is associated with decreases in the  
383 contribution of some of the anthropogenic PM<sub>10</sub> sources. However, using yearly averages for trend analysis may  
384 prevent a proper understanding of the variation in time and of the estimation of the trends based on monthly  
385 averages, which might be more informative, as discussed in section 3.3.



### 3.3. Trends in sources' contributions

#### 3.3.1. Mean rate change in the contribution of PM<sub>10</sub> sources

The source contribution trend analysis was achieved through STL deconvolution (see section 2.6). These trends for all sources over the full period of the study are presented in Table 1. In this table, the part labeled "Rest" represents the difference between the total PM<sub>10</sub> measured mass and the sum of the mass of all PMF-derived factors in order to assess any trend of the unresolved part of PM<sub>10</sub> within our SA study.

PM<sub>10</sub> concentrations present a downward trend from 2013 to 2023, with an average diminution of  $0.73 \mu\text{g m}^{-3} \text{yr}^{-1}$  (3.9%) (S6, Figure S6). Such a downward trend of PM<sub>10</sub> in Grenoble is in line with that observed in other urban sites in Europe (Aas et al., 2024; Borlaza et al., 2022; Caporale et al., 2021; Colette et al., 2021; Gama et al., 2018; Li et al., 2018; Pandolfi et al., 2016). The reduction of PM<sub>10</sub> in Grenoble during this period is significantly larger than that in 30 rural sites of the European Monitoring and Evaluation Programme (EMEP) from 2000 to 2017, which show reductions of PM<sub>10</sub> from  $-0.008$  to  $-0.58 \mu\text{g m}^{-3}$  ( $-1.5\%$  to  $-2.5\%$ ) (Colette et al., 2021). However, the results of our study are highly coherent with results from Aas et al. (2024), presenting a reduction of PM<sub>10</sub> in 2 rural sites in France (La Tardière and Revin) of  $-3.5\% \text{yr}^{-1}$  between 2005 and 2019. Indeed, France is amongst the EU countries with the highest reduction trend, as presented by Aas et al. (2024).

The anthropogenic sources, such as primary traffic, sulfate-rich, and biomass burning, display the highest decrease between 2013 and 2023 in Grenoble, with a reduction of 0.37, 0.25, and  $0.13 \mu\text{g m}^{-3} \text{yr}^{-1}$  (12.9, 6.9, and 5.5%), respectively. The other anthropogenic sources also have a significant decreasing trend; however, they are much lower (nitrate-rich:  $-0.11 \mu\text{g m}^{-3} \text{yr}^{-1}$ , industrial:  $-0.02 \mu\text{g m}^{-3} \text{yr}^{-1}$ ). The downward trends of these anthropogenic sources (mainly traffic, SIA, and industrial) were also underlined for other European urban sites (Colette et al., 2021; Diapouli et al., 2017; Pandolfi et al., 2016). For instance, a similar approach was followed by Pandolfi et al. (2016), investigating the Mann-Kendall trend of PMF-derived sources, and reported an almost equivalent downward trend of the sulfate-rich factor of  $-0.32 \mu\text{g m}^{-3} \text{yr}^{-1}$  between 2004 and 2014 in Spain. The decreasing trends of primary traffic, domestic biomass burning, and industrial emissions are potentially influenced by the reduction in primary emissions due to various abatement strategies (as discussed in the following subsections, notably in 3.3.3 and 3.3.4).

Conversely, natural sources such as mineral dust and chloride-rich factors do not show any significant trend or follow a very weak one (aged sea salt, primary biogenic). MSA-rich is the only source that displays a significant upward trend, with an increase of  $0.08 \mu\text{g m}^{-3} \text{yr}^{-1}$ ; further studies would be needed to relate this last increase to changes in precursor emissions or reactivity during transport. Finally, the low evolutions in the contributions of the natural sources demonstrate that the reduction in PM<sub>10</sub> in Grenoble is essentially related to the reduction of anthropogenic activities, especially sources related to traffic and domestic biomass burning activities.

**Table 1. Trend of PM<sub>10</sub> sources and PM<sub>10</sub> (in  $\mu\text{g m}^{-3} \text{yr}^{-1}$  and  $\% \text{yr}^{-1}$ ).**

	Absolute trend ( $\mu\text{g m}^{-3} \text{yr}^{-1}$ )	Relative trend ( $\% \text{yr}^{-1}$ )	P-values	R <sup>2</sup>
Aged sea salt	-0.01	-2.50	$<<0.01$	0.22
Biomass burning	-0.13	-5.48	$<<0.01$	0.98
Chloride rich	0.00	1.18	0.01	0.07
Industrial	-0.02	-5.36	$<<0.01$	0.40
MSA rich	0.08	6.63	$<<0.01$	0.64



Mineral dust	0.04	1.03	0.02	0.05
Nitrate rich	-0.11	-8.08	<<0.01	0.94
Primary biogenic	-0.01	-0.49	0.03	0.04
Primary traffic	-0.37	-12.85	<<0.01	0.94
Sulfate rich	-0.25	-6.89	<<0.01	0.70
PM <sub>10</sub>	-0.73	-3.89	<<0.01	0.68
Rest	-0.11	-2.13	<<0.01	0.39

420

### 421 3.3.2. Potential influence of meteorology

422 The STL deconvolution is inherently constructed to separate the yearly and seasonal variations from the long-  
 423 term trends. While we discuss the long-term trends of the sources in other sections (3.3.1, 3.3.3, and 3.3.4), it is  
 424 also interesting to evaluate the impact of the meteorology on the seasonal variations of the concentrations. It is  
 425 well known that inversion layers in the lower atmosphere are extremely important for the modulation of the  
 426 concentrations at the ground, particularly in the context of Alpine valleys during winter (Carbone et al., 2010;  
 427 Glojek et al., 2022). In this section, we tried to better evaluate these impacts on the concentrations from the sources  
 428 of PM in the case of our time series.

429 This was considered with the measurements of temperature along the slopes of the mountains very close to the  
 430 city center (as described in section 2.2.3), for the winter periods of 2017-2023. It has been previously shown by  
 431 Allard et al. (2019) that such measurements are representative of the temperature in the valley, despite the potential  
 432 influence of wind slopes. We particularly considered the temperature gradient over the first 700 m above ground  
 433 and the number of days with persistent inversion, as defined in section 2.2.3.

434 The analysis of the relationship between the PM<sub>10</sub> and bulk temperature vertical gradients ( $\Delta T/\Delta z$ ) in winter (Nov,  
 435 Dec, Jan, Feb, Mar), summer (May, June, Jul, Aug), and transition season (remaining months) reveals that thermal  
 436 inversion events and high PM<sub>10</sub> concentration are mainly occurring in winter time (Supplement S7, Figure S8)  
 437 during the 5 years of the study. Periods of persistent temperature inversion were assessed based on the condition  
 438 in Eq. 1, which detected 79 persistent inversion days in series from 4 to 22 consecutive days, for the winter periods  
 439 2017-2023. A meaningful correlation is obtained between PM<sub>10</sub> concentrations and bulk temperature vertical  
 440 gradient ( $r$  reaching 0.60,  $p < 0.001$ ) for these winter months and even better when considering only the persistent  
 441 inversion periods ( $r$  reaching 0.67,  $p < 0.001$ ) for individual years (Table S7).



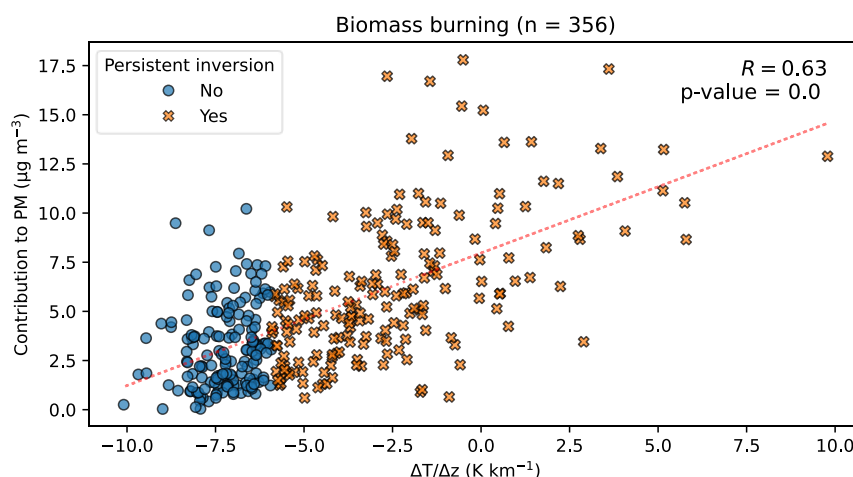


**Figure 5. Daily concentrations of biomass burning to PM<sub>10</sub> and daily temperature gradients ( $\Delta T/\Delta z$ ) during the winter periods (from November to March) of 2017–2023. The dotted red line is the linear regression fit. The blue circle symbols denote days when persistent inversion does not occur, and the orange multiple symbol denotes days when persistent inversion occurs.**

The distribution between the daily PM<sub>10</sub> concentration and daily average  $\Delta T/\Delta z$  in winter months revealed that the majority of PM<sub>10</sub> concentration peaks (in excess of 40  $\mu\text{g m}^{-3}$ ) occur during the persistent inversion days (Figure S9). However, it also shows that a few high PM<sub>10</sub> concentrations could be found on the days without persistent inversion; meanwhile, the days with persistent inversion do not always have high PM<sub>10</sub> concentrations. This result is not surprising since the concentration of PM<sub>10</sub> is not only associated with thermal inversion events but also depends on other meteorological conditions (precipitation, heat deficit) and the variation of pollutant emissions (Carbone et al., 2010; Largeron and Staquet, 2016).

Interestingly, the impact of persistent inversion days on PM<sub>10</sub> concentrations from the residential biomass burning source is larger than that for other sources or total PM<sub>10</sub> (Figure 5), with a higher correlation (0.63). In addition, the contribution of this source is systematically lower during non-inversion days, and large concentrations are essentially made during persistent days. The large impact of the inversions on the local sources is confirmed when comparing the source contribution of the inversion days vs non-inversion days (Figure 6). This figure shows both the large increase in average PM<sub>10</sub> concentrations and also the contributions of the local sources (emissions from residential biomass burning, traffic, industries, mineral dust probably from resuspension) in the cases of inversion days during winter. Conversely, long-range transport sources (sulfate-rich, nitrate-rich) tend to be less important during these inversion days. A similar pattern is observed for the relative contribution of sources to PM (Figure S.10), in which the significant contribution of biomass burning, dust, industrial, and primary traffic is detected during inversion events. The trends of the two most important local anthropogenic sources (domestic biomass burning and traffic) are further discussed in the next sections.

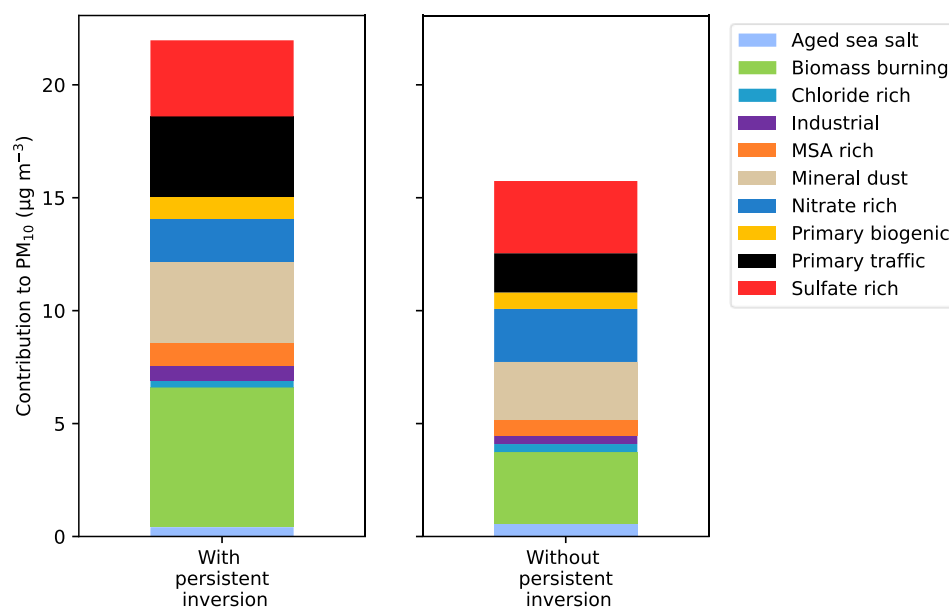


**Figure 6. Contribution of the different sources to the PM<sub>10</sub> composition for days with persistent inversion vs non-inversion days of the winters 2017-2023.**

### 3.3.3. Trend in biomass burning contributions

The trend of the domestic biomass burning PM<sub>10</sub> concentrations is investigated via an STL decomposition analysis on this PMF-derived source (Figure 7), indicating a statistically significant decreasing trend from 2013 to 2023 (p-values <<0.01). The seasonal estimate shows the highest values in the winter season (Nov, Dec, Jan), with a visual trend to a smoothing of the peak concentrations; conversely, from Mar to Sept, the seasonal variations showed constantly lowest values. Extreme residual values were detected in the winter months of 2016, 2017, and 2021, explained by high-concentration episodes of PM<sub>10</sub>, where the concentration exceeded the European standard for PM<sub>10</sub> concentration in 24 hours (PM<sub>10</sub> concentration varied from 50 to 78 µg m<sup>-3</sup>). The linear fit line of the trend is highly significant with R<sup>2</sup> = 0.97, with a reduction of 134 ng m<sup>-3</sup> yr<sup>-1</sup> (-5.5% yr<sup>-1</sup>).

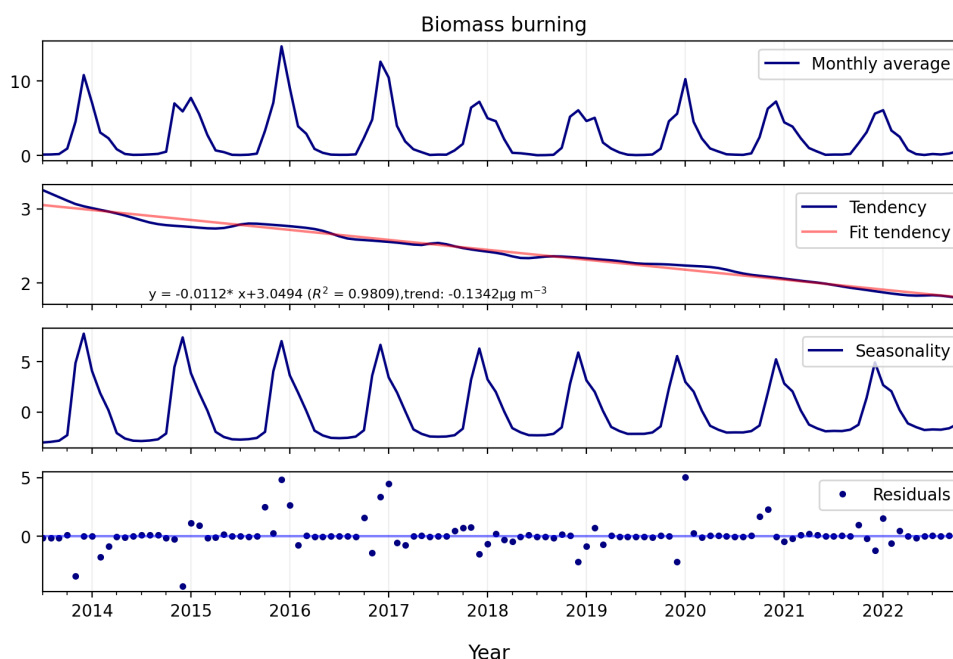
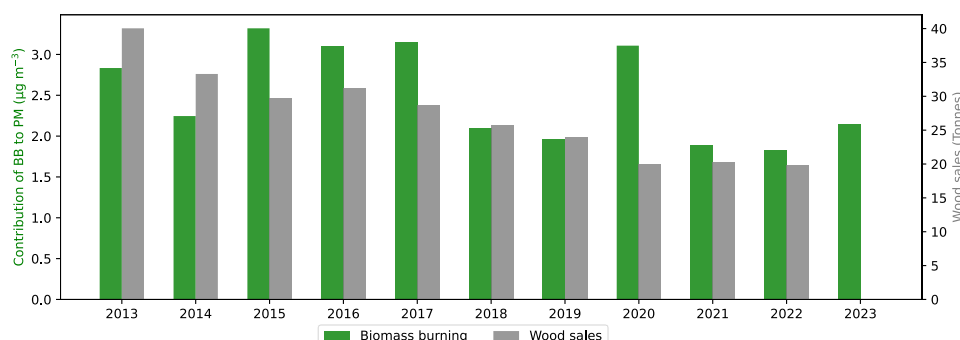


**Figure 7. The season-trend (STL) decomposition of biomass burning**

479  
480

481 This reduction of biomass burning concentrations in Grenoble is 4 times higher than the results from a long-term  
482 study (2012 to 2020) in a French rural site - (Observatoire Pérenne de l'Environnement, OPE) (Borlaza et al.,  
483 2022) - estimated at  $33 \text{ ng m}^{-3} \text{ yr}^{-1}$  over the same period. Besides the study of Borlaza et al. (2022), there are no  
484 previous PMF studies describing any trend of biomass burning factors. Nevertheless, similar trends were found  
485 for concentrations of biomass burning tracers. In particular, Font et al. (2022) presented a downward trend of  
486  $\text{PM}_{10}$  concentration from wood burning (a reduction from 1.5 to 3.8 %  $\text{yr}^{-1}$ ) in urban sites in the United Kingdom  
487 from 2010 to 2021, by calculating the emission of wood burning from aethalometer measurement. Similarly, from  
488 2002 to 2018 in Norway, a downward trend of 2.8%  $\text{yr}^{-1}$  was also detected for levoglucosan (Espen Yttri et al.,  
489 2021). Additionally, Colette et al. (2021) modeled the trend of the emissions from different activities in Europe,  
490 showing that the trend of  $\text{PM}_{10}$  heating emissions was decreasing in the period 2000-2017, with mean rate values  
491 varying from 0.8 to 3.3%  $\text{yr}^{-1}$  for 30 European countries (EMEP monitoring sites). Even though the chemicals  
492 and the period of these studies differ, a decreasing trend is generally observed among European cities, including  
493 the one investigated here. Interestingly, the biomass burning source in Grenoble shows the strongest decreasing  
494 trend, with a reduction of 5.5%  $\text{yr}^{-1}$ .

495 Since the biomass burning sources in Grenoble are related to residential heating, the observed reduction of the  
496 concentrations from this source could be linked to household behaviors (including appliance renovation) on top  
497 of the changes in meteorological conditions, lowering the overall heating demand. The average annual biomass  
498 burning sources PMF-derived is compared to the local  $\text{PM}_{10}$  emission inventory for residential heating (tonnes)  
499 in the Grenoble metropolis, estimated by the regional air quality monitoring agency (Atmo AuRA), to confirm  
500 the trend of biomass burning (Figure 8). This emission inventory has been available until 2022.



501  
502 **Figure 8. Comparison between annual average PM<sub>10</sub> emission inventory based on the quantity of wood sales (in grey)**  
503 **in the Grenoble metropolis and the yearly average PM<sub>10</sub> concentrations from the PMF biomass burning factor (in**  
504 **green).**

505 Except for the year 2020, the annual average of biomass burning agreed with the emission inventory,  
506 demonstrating the consistency between the sources observed by the PMF model and the local inventory emission  
507 data. Since 2015, the Grenoble metropolis has set up an air-wood bonus to encourage households to renew their  
508 individual wood-burning appliance (fireplace or stove). It aims to replace all open fireplaces with closed  
509 appliances in October 2024. The downward trend of biomass burning concentration could then be considered as  
510 partly due to the implementation of dedicated action plans at the regional scale.

### 511 3.3.4. Trends in traffic exhaust emissions

512 Similar to the time series of biomass burning concentrations, the traffic contribution was subjected to specific  
513 STL analysis (Figure 9). A significant downward trend of the concentrations of PM from traffic emission is  
514 detected with a reduction of  $374 \text{ ng m}^{-3} \text{ yr}^{-1}$  ( $12.9\% \text{ yr}^{-1}$ ) ( $p\text{-value} \ll 0.01$ ). This reduction is almost 3 times larger  
515 than that of the biomass burning concentrations. Traffic concentration before 2017 also showed a clear seasonality  
516 with maxima in winter, which nearly disappeared from 2018 onward. It is striking that the same behaviors (strong  
517 downward trend and smoothing) are also observed for NO<sub>x</sub> concentration, another indicator of traffic exhaust  
518 emission, which is also observed for NO<sub>x</sub> seasonal patterns (see Supplement S6 and Figure S7). Residuals show  
519 extreme values in the same month as biomass burning in 2016 and 2017, matching the PM<sub>10</sub> episode. The traffic  
520 trend closely follows a linear regression fit line, with  $R^2 = 0.94$ .

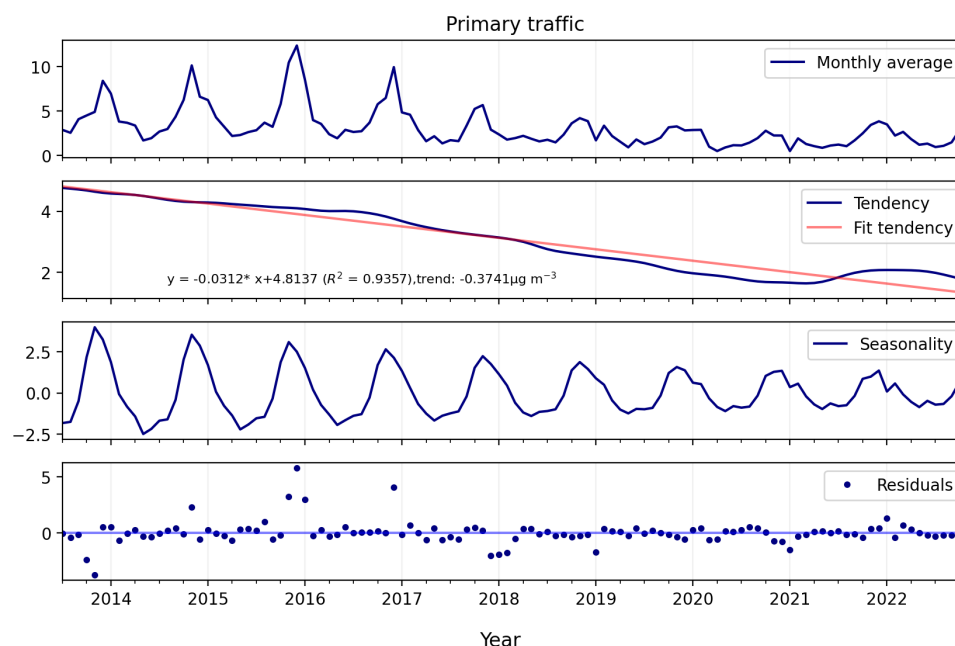


**Figure 9. The season-trend (STL) decomposition of PMF-derived traffic source**

The downward traffic trend observed in this study is consistent with another long-term study (2012–2020) of a rural site in France, which showed a traffic trend of  $-0.1 \mu\text{g m}^{-3} \text{ yr}^{-1}$  (Borlaza et al., 2022). This is aligned with other results of fossil fuel black carbon in several rural sites in France (Font et al., 2025), or EC over many rural sites in Europe (Aas et al., 2024). Additionally, our result also agrees with other studies, like that by Pandolfi et al. (2016), which indicated a downward trend of traffic sources in an urban site in Spain, with a reduction of  $0.11 \mu\text{g m}^{-3} \text{ yr}^{-1}$ , which is lower than that of our study. Finally, the trend of traffic emission to  $\text{PM}_{10}$  in 30 European countries was modeled as reported by Colette et al. (2021), showing a downward trend with a reduction from 2.3 to  $3.5\% \text{ yr}^{-1}$  from 2000 to 2017. As for biomass burning, the Grenoble supersite seems then experiencing faster reductions in primary traffic PM loadings than most of others European cities.

Furthermore, the PMF-derived traffic factor was compared to the local  $\text{PM}_{10}$  traffic emission inventory by fuel type (provided by Atmo AuRA), revealing very similar trends (Figure 10). In addition, this source is also compared to the  $\text{PM}_{10}$  emission by the transport sector (kilotonnes) over France, which was assessed from the emission inventory data of CITEPA (Figure S11), also confirming the concomitant reductions of traffic emissions and contributions to  $\text{PM}_{10}$  in ambient air.

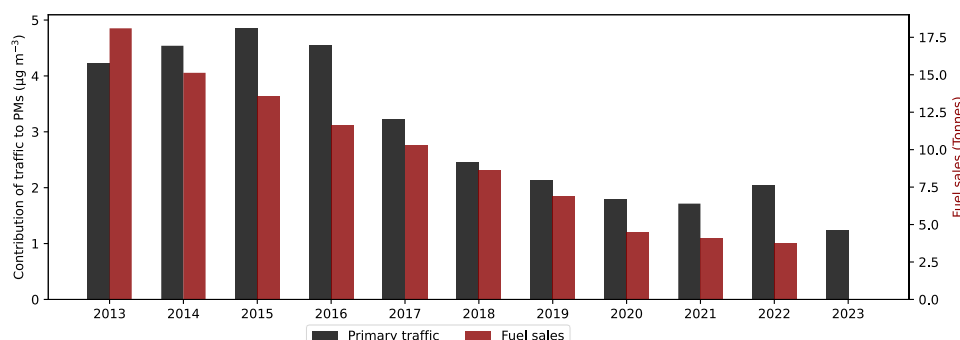


**Figure 10. Comparison between annual average PM<sub>10</sub> emission inventory based on the quantity of fuel sale (red bar) in the Grenoble metropolis and the yearly average PM<sub>10</sub> concentrations from the PMF-derived traffic source contributions (black bar).**

This traffic trend may be separated into three parts. Between 2014 and 2016 with a slow decrease trend of -3% yr<sup>-1</sup>; from 2016 to 2021, with an average reduction of 10% yr<sup>-1</sup>, and a mild increasing trend of approximately 3% yr<sup>-1</sup> in the last three years of the study. The beginning of this increase coincides with the post-lockdown period, when transportation activities were back to normal, resulting in a fairly similar contribution of traffic sources compared to that in the pre-lockdown period.

Besides the implementation of the two versions of the Euro 6 emission standards (introduced in 2015 and 2018, respectively), local emission abatement strategies decided by Grenoble municipality from 2016 onwards might be the main drivers for the observed decreasing trends (City's low emission zone <https://zfe.grenoblealpesmetropole.fr/> last assessed: 21/05/2025).

### 3.4. Trends in PM<sub>10</sub> OP sources

In this section, the sources of OP are assessed using regression techniques, which are presented in section 2.6. The most appropriate model is selected based on characteristics of PMF-derived sources and OP<sub>v</sub>, as shown in section 3.4.1. Intrinsic OP derived from the best regression model, indicating the highest redox-active PM sources, is presented in section 3.4.2. Finally, section 3.4.3 provides the trend of OP sources, highlighting which sources are the drivers of OP trends.

#### 3.4.1. Selection of the most appropriate model

Following the methodology exposed in Ngoc Thuy et al. (2024), the characteristics of the dataset, including collinearity and heteroscedasticity, are tested in order to select a satisfactory inversion model for OP<sub>DTT</sub> source apportionment (SA) and OP<sub>AA</sub> SA (Table S8). The OP SA can be applied for the 11-year PMF solution since the source profiles have been demonstrated to be homogenous over the years. Consequently, the OP<sub>m</sub> should be substantially homogenous over the years (Ngoc Thuy et al., 2024), and it is unnecessary to perform the OP SA for each year separately. The characteristic tests indicate that the weighted positive least squares (wPLS) and weighted least squares (WLS) could be suitable models for both OP<sub>AA</sub> and OP<sub>DTT</sub> SA. The average accuracy metrics of the testing dataset in 500 iteration runs (including R<sup>2</sup>, RMSE, MAE) of wPLS and WLS were compared to select the most appropriate model (Table S9). Finally, WLS was chosen due to the highest R<sup>2</sup> and lowest error for both OP<sub>AA</sub> and OP<sub>DTT</sub> prediction. The comparison between observed and predicted OP<sub>AA</sub> and OP<sub>DTT</sub> showed





a good correlation between measured OP and WLS predicted OP, with  $R^2 = 0.80$  and  $0.70$  for  $OP_{AA}$  and  $OP_{DTT}$ , respectively (Figure S12 and S13), with  $n = 1570$  for  $OP_{AA}$  and  $OP_{DTT}$ . In addition, the study revealed good performance of MLP and RF for the training and testing datasets (Table S10). These neural network models were overfitting the results of OP SA for the 6 French sites tested in Ngoc Thuy et al. (2024) since the number of samples was lower than 200 for individual sites. The present study confirmed the conclusion of Ngoc Thuy et al. (2024), demonstrating that a higher number of samples improved the performance of the neural network model. However, such non-linear models do not provide values for intrinsic OP, and cannot be selected for the final results at this stage.

### 3.4.2. Intrinsic OP of PMF-derived sources

The intrinsic OP of  $1\mu\text{g PM}_{10}$  source ( $OP^m \text{ nmol min}^{-1} \mu\text{g}^{-1}$ ) is investigated thanks to the WLS technique, resulting in 500 values of  $OP^m$  for each source (Table 2 and Table S11). The anthropogenic sources, including biomass burning, industrial, and traffic, have the dominant intrinsic  $OP_{DTT}$  and  $OP_{AA}$ , which is consistent with the study in 2017-2018 in Grenoble (Borlaza, 2021) and results obtained at other French sites (Ngoc Thuy et al., 2024; Weber et al., 2021) and EU sites (Fadel et al., 2023; Veld et al., 2023). The different ranking of the intrinsic OP of the sources according to the two assays is also aligned with previous results (Weber et al., 2021). While intrinsic  $OP_{AA}$  of biomass burning is highest ( $0.76 \text{ nmol min}^{-1} \mu\text{g}^{-1}$ ), followed by industrial ( $0.48 \text{ nmol min}^{-1} \mu\text{g}^{-1}$ ) and traffic ( $0.38 \text{ nmol min}^{-1} \mu\text{g}^{-1}$ ), the order of intrinsic  $OP_{DTT}$  is industrial ( $0.52 \text{ nmol min}^{-1} \mu\text{g}^{-1}$ ), traffic ( $0.38 \text{ nmol min}^{-1} \mu\text{g}^{-1}$ ) and biomass burning ( $0.14 \text{ nmol min}^{-1} \mu\text{g}^{-1}$ ). The intrinsic  $OP_{DTT}$  of biomass burning is also lower than that of  $OP_{AA}$ , as reported by Borlaza et al. (Borlaza et al., 2021), suggesting the synergistic and antagonistic effects between some elements, quinones, or bioaerosols, decreasing the overall intrinsic  $OP_{DTT}$  of this source (Pietrogrande et al., 2022; Samake et al., 2017; Xiong et al., 2017). The other anthropogenic sources, including nitrate-rich and sulfate-rich, have lower intrinsic OP than anthropogenic sources associated with combustion (traffic and biomass burning), as reported by Daellenbach et al. (2020). The natural sources have a negligible intrinsic OP (lower than  $0.03 \text{ nmol min}^{-1} \mu\text{g}^{-1}$ ). These findings highlight the high impact of the anthropogenic sources, verified for the overall period 2013-2023.

**Table 2. Intrinsic  $OP_{AA}$  and  $OP_{DTT}$  ( $\text{nmol min}^{-1} \mu\text{g}^{-1}$ ) of  $\text{PM}_{10}$  sources (mean  $\pm$  std of 500 iterations)**

Source	$OP_{AA}$	$OP_{DTT}$
Aged sea salt	$-0.02 \pm 0.07$	$0.03 \pm 0.02$
Biomass burning	$0.76 \pm 0.13$	$0.14 \pm 0.09$
Chloride rich	$-0.07 \pm 0.09$	$0.01 \pm 0.02$
Industrial	$0.48 \pm 0.14$	$0.52 \pm 0.08$
MSA rich	$0.20 \pm 0.04$	$0.01 \pm 0.02$
Mineral dust	$-0.03 \pm 0.06$	$0.01 \pm 0.02$
Nitrate rich	$0.09 \pm 0.16$	$0.11 \pm 0.12$
Primary biogenic	$0.00 \pm 0.04$	$0.02 \pm 0.03$
Primary traffic	$0.38 \pm 0.10$	$0.24 \pm 0.07$
Sulfate rich	$-0.01 \pm 0.08$	$0.09 \pm 0.04$



### 3.4.3. Trends in OP

The trend of OP is first presented by the yearly average contribution of sources to  $OP_{AA}$  and  $OP_{DTT}$  (Figure 4), indicating a reduction of OP values over the years. Overall, the yearly average of the  $OP_{AA}^v$  and  $OP_{DTT}^v$  is decreasing and reached its lowest values in 2021 ( $2.41$  and  $1.17$   $\text{nmol min}^{-1} \text{m}^{-3}$  for  $OP_{AA}$  and  $OP_{DTT}$ , respectively). From 2018 onward, both assays consistently exhibited lower  $OP^v$  values than in preceding years. Although  $OP^v$  is normalized to  $PM_{10}$  mass concentration, implying that a decrease in  $PM_{10}$  concentration generally reduces  $OP^v$ , the contribution of sources to OP is different from that of  $PM_{10}$ . While dust and sulfate-rich are dominantly contribute to  $PM_{10}$ , biomass burning is the most important contributor to  $OP_{AA}$  ( $1.87 \pm 2.7$   $\text{nmol min}^{-1} \text{m}^{-3}$ ), and primary traffic is commonly assessed as the largest contributor to  $OP_{DTT}$  ( $0.71 \pm 0.70$   $\text{nmol min}^{-1} \text{m}^{-3}$ ). The industrial mass contribution is 10 times lower than that of the sulfate-rich. However, industrial emissions appear to contribute much more to  $OP_{AA}$  and equally to  $OP_{DTT}$  than the sulfate-rich factor. This finding was also observed in 2017-2018 at the same site in Grenoble (Borlaza, 2021). This significant contribution of traffic and biomass burning over the years is more evident when considering relative contribution (Figure S15). These results again emphasize the importance of considering not only the mass concentration but also its redox activity in evaluating the potential adverse health effects of a source of PM.

In addition, the temporal evolution of  $OP_{AA}$  and  $OP_{DTT}$  did not exactly follow  $PM_{10}$  trends, especially for the period of 2016-2017 and 2019-2020. Regarding the period between 2016 and 2017, a dramatic increase in  $PM_{10}$  concentration is observed, principally due to the higher contribution of nitrate and sulfate-rich. On the other hand,  $OP_{AA}$  and  $OP_{DTT}$  values remained fairly unchanged between 2016 and 2017. Focus on 2019 and 2020, the  $PM$  concentration and  $OP^v$  values are identical (less than  $0.001$   $\mu\text{g m}^{-3}$  and  $\text{nmol min}^{-1} \text{m}^{-3}$  of difference, respectively), while  $OP_{AA}^v$  presents a remarkable difference ( $\Delta = 0.8$   $\text{nmol min}^{-1} \text{m}^{-3}$ ). Indeed, the discrepancy between 2019 and 2020 in  $OP_{AA}^v$  is principally attributable to a higher contribution to biomass burning, which is the dominant driver of  $OP_{AA}^v$ . Overall, the downward trend of  $OP_{AA}$  and  $OP_{DTT}$  is different from  $PM_{10}$ , since the driven sources of OP and PM are different.

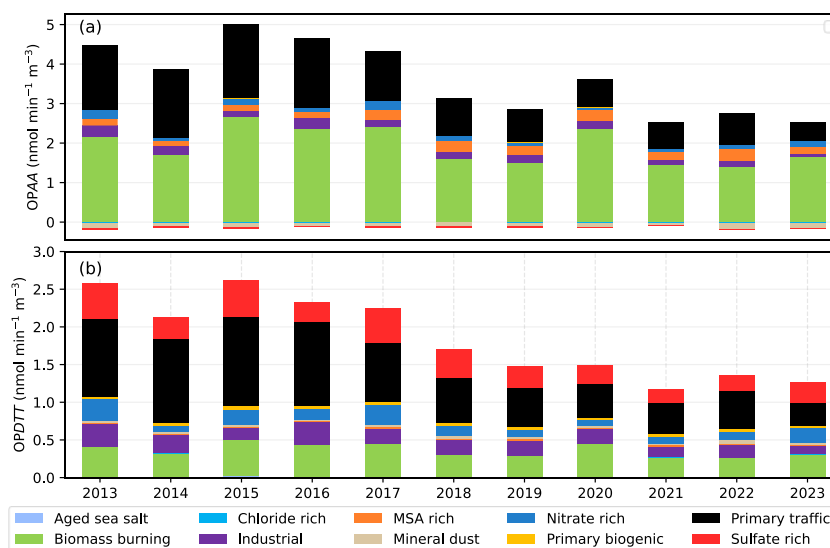


Figure 11. Yearly average contribution of sources to (a)  $OP_{AA}^v$  and (b)  $OP_{DTT}^v$



619 The yearly average may not be properly representative of the trends of OP; therefore, a STL deconvolution was  
620 performed for  $OP_{AA}^m$  and  $OP_{DTT}^m$  (Figures S16, S17, respectively) to investigate the trend of  $OP^m$  over the 11  
621 years of the study. Indeed, considering the trend of the intrinsic  $OP^m$  confirms that the downward trend of some  
622 sources leads to a change in the trend of  $OP_{AA}^m$  and  $OP_{DTT}^m$ .

623 An insignificant linear trend is observed for  $OP_{AA}^m$  (fit line:  $R^2 = 0.4$ , p-values  $<< 0.01$ ), yet its average intrinsic  
624 activity still exhibits a decreasing value, with the annual mean falling by approximately  $0.002 \text{ nmol min}^{-1} \text{ m}^{-3}$   
625 (2.5 %) across the study period. Interestingly, the seasonality of  $OP_{AA}^m$  exactly matches the seasonality of  
626 biomass-burning concentrations, pointing out that the high values of  $OP_{AA}^m$  in winter align with biomass-burning  
627 activities. The trend line of  $OP_{AA}^m$  did not match the trend of biomass burning nor that of the traffic or industrial  
628 emissions, suggesting the synergistic effect between sources, as well as the influence of the other sources outside  
629 of the winter season, such as MSA-rich and primary biogenic, which get a high ranking of  $OP_{AA}^m$  (Table 2).

630 Conversely, the  $OP_{DTT}^m$  showed a significant downward trend ( $R^2 = 0.6$ , p-value  $<< 0.01$ ), with a reduction of  $0.005$   
631  $\text{nmol min}^{-1} \mu\text{g}^{-1}$  (6.5%) across 11 years. The seasonality of  $OP_{DTT}^m$  is different from that of biomass burning and  
632  $OP_{AA}^m$ , since biomass burning is not the main driver of  $OP_{DTT}^m$  (only ranked third), indicating a lower influence of  
633 this source on  $OP_{DTT}^m$  compared to  $OP_{AA}^m$ . Interestingly, a slight increase in  $OP_{DTT}^m$  from 2021 onward is also  
634 observed, which is associated with  $PM_{10}$  and traffic, suggesting that traffic emission could be the main driver for  
635 increasing  $PM_{10}$  concentration and  $OP_{DTT}^m$  from 2021. Overall, the relative decrease of  $OP_{DTT}^m$  exceeds that of  
636  $OP_{AA}^m$  could be explained by the 4<sup>th</sup> most important contributor to these OPs. All four leading contributors to  
637  $OP_{DTT}^m$  show significant reductions, whereas MSA-rich factor, one of the top four contributors to  $OP_{AA}^m$ , has an  
638 increasing trend. These findings again underscore that trends in  $OP^m$  are governed by the evolution of the sources  
639 most active in each assay. Thus, the decrease in the magnitude of the  $OP^m$  depends on how its dominant redox-  
640 active sources evolve over time.

641 Considering the volume-based metrics ( $OP_v$ ), a downward trend is detected for  $OP_{AA}$  and  $OP_{DTT}$ .  $PM_{10}$  decreased  
642 by 3.9 % over the decade, which is consistently comparable to  $OP_{AA}^v$  (4.9 %) and  $OP_{DTT}^v$  (5.3 %). This good  
643 agreement partially reflects the influence of the PM mass concentration since these  $OP^v$  values are normalized to  
644  $PM_{10}$  mass concentration. However, the slight difference in the relative downward trend could be related to the  
645 most driven sources of OP and PM, as discussed above.

646 Finally, the impact of persistent inversion days on the  $OP^v$  is also investigated to assess the association between  
647 the redox activity of PM sources and thermal inversion. A comparison of the source's contribution to  $OP^v$  (for  
648 both AA and DTT) between the period with and without persistent inversions is carried out and shown in Figure  
649 S14. The comparison confirms the larger increases in average  $OP_{AA}$  (85.1%) and  $OP_{DTT}$  (63.8 %) compared to  
650 that of  $PM_{10}$  (39.6%) for the persistent inversion periods. The higher values of  $OP_{AA}$  and  $OP_{DTT}$  are related to the  
651 larger increases in the contribution of local anthropogenic sources, with BB impacting most the  $OP_{AA}$  values while  
652 traffic significantly influences  $OP_{DTT}$ . This result again highlights the potential effect of persistent inversion on  
653 the  $PM_{10}$  source's contribution, but all the more of their redox-active properties, which could be associated with  
654 the health-relevant metrics (Tassel et al., 2025 in progress).

655 Over the decade, anthropogenic sources have driven OP, with biomass burning impacting  $OP_{AA}$  and traffic/  
656 industrial sources dominating  $OP_{DTT}$ . Frequent thermal inversion in Alpine valley strongly amplifies OP, which is  
657 more significant than the mass of  $PM_{10}$  itself. Finally,  $OP_v$  and intrinsic OP trends over the decade do not align



with that of PM<sub>10</sub> mass, emphasizing the need to prioritize redox-active components over the bulk PM concentration in air quality policy.

#### 4. Conclusions

Thanks to long-term PM<sub>10</sub> observations with a detailed set of chemical markers, a comprehensive source apportionment was performed to identify the evolution of PM<sub>10</sub> sources in Grenoble (France). This is one of the very few studies in Europe that could assess over 11 years of PM<sub>10</sub> sources and the only study so far investigating trends in PM<sub>10</sub>-related OP. The trend of PM<sub>10</sub> sources, especially anthropogenic sources such as biomass burning and primary traffic, was evaluated and linked to the meteorology and emission reduction policies. In addition, the trend of OP<sup>m</sup>, OP<sup>v</sup>, and sources of OP revealed that the trend of OP depends on the source that drives OP. The analysis of these trends confirms the improvement of the air quality at the Grenoble supersite from 2013 to 2023, and objectivates the main sources that are involved in their concentration' decrease.

Nevertheless, the following methodological limitations in this long-term study shall be kept in mind:

- Daily concentrations of metal elements were only analyzed for some periods (2013, 2017-2018, 2020-2021), while the remaining data were derived from weekly sampling. An imputation technique was implemented to impute daily concentrations. The PMF result demonstrated the stability of most chemical profiles at Grenoble from 2013 to 2023, compared to those previously published (Borlaza et al., 2021), despite these uncertainties in the imputed metal concentrations.

- The process of implementing such a PMF analysis strategy is not straightforward. A combined PMF approach could be used for datasets with different time resolution (Via et al., 2023). This approach would allow combining the 7-day and daily filter samples into a PMF without performing imputation.

- The lack of a secondary biogenic organic aerosol tracer in long-term observations prevents the identification of the BSOA source, which could make up about 10% of the total mass of PM<sub>10</sub> on a yearly average, as observed in previous work at the site (Borlaza et al., 2021), which used 3-MBTCA and picnic acid for the yearly period of observation.

Overall, a total of ten sources were identified, including aged sea salt, biomass burning, chloride-rich mineral dust, MSA-rich, nitrate-rich, industrial, primary biogenic, and primary traffic. The source chemical profiles are consistent with those presented in 2017-2018 (Borlaza et al., 2021), demonstrating that the sources of PM<sub>10</sub> in Grenoble were relatively stable during our study period. The trend of PM<sub>10</sub> sources was investigated using STL decomposition, which reveals a downward trend for all the PM<sub>10</sub> sources over 11 years, especially for the anthropogenic sources. Extending PMF outputs to oxidative potential apportionment showed that biomass burning, traffic, and industrial emissions dominate redox activity in both the ascorbic acid (AA) and dithiothreitol (DTT) assays. Trend analysis of volume- and mass-normalized OP metrics indicates that biomass burning governs the long-term behavior of OP<sub>AA</sub>. In contrast, traffic is the principal driver of OP<sub>DTT</sub> assay, underscoring source-specific control of PM<sub>10</sub> OP in the Grenoble atmosphere.

Both of these anthropogenic sources, as well as their influences on PM<sub>10</sub> OP, showed significant decreasing trends concomitantly to the implementation of emission reduction strategies (both at the national and regional levels) that should be reinforced to reach the goals of the European zero pollution action plan and the recently revised Directive on ambient air quality (2024/2881/EU). The continuation of these measurements will take place in the coming years, with this site being selected as one of the supersites for the new EU Air Quality directive.



697 **Data availability**

698 The datasets could be made available upon request by contacting the corresponding authors.

699 **Author contributions**

700 VDNT performed the source apportionment and the trend of sources, and the result visualisation. GU, JLJ  
701 mentoring, supervision, validation of the methodology and results. RE, SD, CV, and AN contributed to data  
702 acquisition (analytical investigation on samples) and data curation. OF, JLJ, and GU acquired funding for the  
703 original PM sampling and analysis. VDNT wrote the original draft. All authors reviewed and edited the  
704 manuscript.

705 **Competing interests**

706 The authors declare that they have no conflict of interest.

707 **Acknowledgment**

708 The authors would like to express their sincere gratitude to many people of the Air-O-Sol analytical platform at  
709 IGE for sample management and chemical analyses. We gratefully acknowledge the personnel at Atmo AuRA  
710 (C. Bret, C. Chabanis) for their support in conducting the dedicated sample collection and providing weekly metals  
711 data.

712 **Financial support**

713 This study was partially funded by the French Ministry of Environment through its contributions to the CARA  
714 program. Part of the project was also funded by Atmo AuRA (ensuring filter sampling and costs related to the  
715 analyses of the elemental concentrations in the weekly samples. IGE contributed financially to the analyses of  
716 ions. The extended analyses for the daily trace elements were funded by the QAMECS program from Ademe  
717 (1662C0029).

718



719 **Reference**

- 720 Aas, W., Fagerli, H., Alastuey, A., Cavalli, F., Degorska, A., Feigenspan, S., Brenna, H., Gliß, J., Heinesen, D.,  
721 Hueglin, C., Holubová, A., Jaffrezo, J.-L., Mortier, A., Murovec, M., Putaud, J.-P., Rüdiger, J., Simpson, D.,  
722 Solberg, S., Tsyro, S., Tørseth, K., and Yttri, K. E.: Trends in Air Pollution in Europe, 2000–2019, *Aerosol and*  
723 *Air Quality Research*, 24, 230237, <https://doi.org/10.4209/aaqr.230237>, 2024.
- 724 Allard, J., Chevrier, F., Laurent, J.-P., Coulaud, C., Paci, A., Jezek, I., Mocnik, G., Brulfert, G., Besombes, J.-L.,  
725 and Jaffrezo, J.-L.: Un système de mesure de température pour suivre l'influence de la stabilité atmosphérique sur  
726 la qualité de l'air dans la vallée de l'Arve, *Météorologie*, 39, <https://doi.org/10.4267/2042/70368>, 2019.
- 727 Ayres, J. G., Borm, P., Cassee, F. R., Castranova, V., Donaldson, K., Ghio, A., Harrison, R. M., Hider, R., Kelly,  
728 F., Kooter, I. M., Marano, F., Maynard, R. L., Mudway, I., Nel, A., Sioutas, C., Smith, S., Baeza-Squiban, A.,  
729 Cho, A., Duggan, S., and Froines, J.: Evaluating the toxicity of airborne particulate matter and nanoparticles by  
730 measuring oxidative stress potential - A workshop report and consensus statement, *Inhalation Toxicology*, 20, 75–  
731 99, <https://doi.org/10.1080/08958370701665517>, 2008.
- 732 Azur, M. J., Stuart, E. A., Frangakis, C., and Leaf, P. J.: Multiple imputation by chained equations: what is it and  
733 how does it work?, *International journal of methods in psychiatric research*, 20, 40–49,  
734 <https://doi.org/10.1002/mpr.329>, 2011.
- 735 Baduel, C., Voisin, D., and Jaffrezo, J.-L.: Water-soluble atmospheric HULIS in urban environments Water-  
736 soluble atmospheric HULIS in urban environments Water-soluble atmospheric HULIS in urban environments,  
737 *Chem. Phys. Discuss*, 2009.
- 738 Baduel, C., Nozière, B., and Jaffrezo, J. L.: Summer/winter variability of the surfactants in aerosols from  
739 Grenoble, France, *Atmospheric Environment*, 47, 413–420, <https://doi.org/10.1016/j.atmosenv.2011.10.040>,  
740 2012.
- 741 Bates, J. T., Weber, R. J., Verma, V., Fang, T., Ivey, C., Liu, C., Sarnat, S. E., Chang, H. H., Mulholland, J. A.,  
742 and Russell, A.: Source impact modeling of spatiotemporal trends in PM<sub>2.5</sub> oxidative potential across the eastern  
743 United States, *Atmospheric Environment*, 193, 158–167, <https://doi.org/10.1016/j.atmosenv.2018.08.055>, 2018.
- 744 Belis, C. A., Favez, O., Harrison, R. M., Larsen, B. R., Amato, F., El Haddad, I., Hopke, P. K., Nava, S., Paatero,  
745 P., Prévôt, A., Quass, U., Vecchi, R., Viana, M., and European Commission (Eds.): European guide on air  
746 pollution source apportionment with receptor models, Publications Office, Luxembourg, 1 pp.,  
747 <https://doi.org/10.2788/9332>, 2014.
- 748 Belis, C. A., Karagulian, F., Amato, F., Almeida, M., Artaxo, P., Beddows, D. C. S., Bernardoni, V., Bove, M.  
749 C., Carbone, S., Cesari, D., Contini, D., Cuccia, E., Diapouli, E., Eleftheriadis, K., Favez, O., El Haddad, I.,  
750 Harrison, R. M., Hellebust, S., Hovorka, J., Jang, E., Jorquera, H., Kammermeier, T., Karl, M., Lucarelli, F.,  
751 Mooibroek, D., Nava, S., Nøjgaard, J. K., Paatero, P., Pandolfi, M., Perrone, M. G., Petit, J. E., Pietrodangelo, A.,  
752 Pokorná, P., Prati, P., Prevot, A. S. H., Quass, U., Querol, X., Saraga, D., Sciare, J., Sfetsos, A., Valli, G., Vecchi,  
753 R., Vestenius, M., Yubero, E., and Hopke, P. K.: A new methodology to assess the performance and uncertainty  
754 of source apportionment models II: The results of two European intercomparison exercises, *Atmospheric*  
755 *Environment*, 123, 240–250, <https://doi.org/10.1016/j.atmosenv.2015.10.068>, 2015.
- 756 Borlaza: Disparities in particulate matter (PM<sub>10</sub>) origins and oxidative potential at a city scale (Grenoble, France)  
757 - Part 2: Sources of PM<sub>10</sub> oxidative potential using multiple linear regression analysis and the predictive  
758 applicability of multilayer perceptron n, *Atmospheric Chemistry and Physics*, 21, 9719–9739,  
759 <https://doi.org/10.5194/acp-21-9719-2021>, 2021.
- 760 Borlaza, L., Weber, S., Uzu, G., Jacob, V., Cañete, T., Micallef, S., Trébuchon, C., Slama, R., Favez, O., and  
761 Jaffrezo, J.-L.: Disparities in particulate matter (PM<sub>10</sub>) origins and oxidative potential at a city scale (Grenoble,  
762 France) - Part 1: Source apportionment at three neighbouring sites, *Atmospheric Chemistry and Physics*, 21, 5415–  
763 5437, <https://doi.org/10.5194/acp-21-5415-2021>, 2021.
- 764 Borlaza, L., Weber, S., Marsal, A., Uzu, G., Jacob, V., Besombes, J. L., Chatain, M., Conil, S., and Jaffrezo, J.  
765 L.: Nine-year trends of PM<sub>10</sub> sources and oxidative potential in a rural background site in France, *Atmospheric*  
766 *Chemistry and Physics*, 22, 8701–8723, <https://doi.org/10.5194/acp-22-8701-2022>, 2022.





- 767 Borlaza-Lacoste, L., Mardoñez, V., Marsal, A., Hough, I., Dinh, N. T. V., Dominutti, P., Jaffrezo, J.-L., Alastuey,  
768 A., Besombes, J.-L., Močnik, G., Moreno, I., Velarde, F., Gardon, J., Cornejo, A., Andrade, M., Laj, P., and Uzu,  
769 G.: Oxidative potential of particulate matter and its association to respiratory health endpoints in high-altitude  
770 cities in Bolivia, *Environmental Research*, 255, 119179, <https://doi.org/10.1016/j.envres.2024.119179>, 2024.
- 771 Brighty, A., Jacob, V., Uzu, G., Borlaza, L., Conil, S., Hueglin, C., Grange, S. K., Favez, O., Trébuchon, C., and  
772 Jaffrezo, J. L.: Cellulose in atmospheric particulate matter at rural and urban sites across France and Switzerland,  
773 *Atmospheric Chemistry and Physics*, 22, 6021–6043, <https://doi.org/10.5194/acp-22-6021-2022>, 2022.
- 774 Calas, A., Uzu, G., Martins, J. M. F., Voisin, Di., Spadini, L., Lacroix, T., and Jaffrezo, J. L.: The importance of  
775 simulated lung fluid (SLF) extractions for a more relevant evaluation of the oxidative potential of particulate  
776 matter, *Scientific Reports*, 7, 1–12, <https://doi.org/10.1038/s41598-017-11979-3>, 2017.
- 777 Calas, A., Uzu, G., Kelly, F. J., Houdier, S., Martins, J. M. F., Thomas, F., Molton, F., Charron, A., Dunster, C.,  
778 Ollie, A., Jacob, V., Besombes, J. L., Chevrier, F., and Jaffrezo, J. L.: Comparison between five acellular  
779 oxidative potential measurement assays performed with detailed chemistry on PM10 samples from the city of  
780 Chamonix (France), *Atmospheric Chemistry and Physics*, 18, 7863–7875, [https://doi.org/10.5194/acp-18-7863-](https://doi.org/10.5194/acp-18-7863-2018)  
781 2018, 2018.
- 782 Caporale, G. M., Gil-Alana, L. A., and Carmona-González, N.: Particulate matter 10 (PM10): persistence and  
783 trends in eight European capitals, *Air Quality, Atmosphere and Health*, 14, 1097–1102,  
784 <https://doi.org/10.1007/s11869-021-01002-0>, 2021.
- 785 Carbone, C., Decesari, S., Mircea, M., Giulianelli, L., Finessi, E., Rinaldi, M., Fuzzi, S., Marinoni, A., Duchi, R.,  
786 Perrino, C., Sargolini, T., Vardè, M., Sprovieri, F., Gobbi, G. P., Angelini, F., and Facchini, M. C.: Size-resolved  
787 aerosol chemical composition over the Italian Peninsula during typical summer and winter conditions,  
788 *Atmospheric Environment*, 44, 5269–5278, <https://doi.org/10.1016/j.atmosenv.2010.08.008>, 2010.
- 789 Colette, A., Solberg, S., Aas, W., and Walker, S.-E.: Understanding Air Quality Trends in Europe, 2021.
- 790 Craney, T. A. and Surles, J. G.: Model-dependent variance inflation factor cutoff values, *Quality Engineering*, 14,  
791 391–403, <https://doi.org/10.1081/QEN-120001878>, 2002.
- 792 Daellenbach, K. R., Uzu, G., Jiang, J., Cassagnes, L.-E., Leni, Z., Vlachou, A., Stefanelli, G., Canonaco, F.,  
793 Weber, S., Segers, A., and Sources, al: Sources of particulate-matter air pollution and its oxidative potential in  
794 Europe of particulate-matter air pollution and its oxidative potential in Europe, *Nature*, 587,  
795 <https://doi.org/10.1038/s41586-020-2902-8>, 2020.
- 796 Diapouli, E., Manousakas, M., Vratolis, S., Vasilatou, V., Maggos, T., Saraga, D., Grigoratos, T., Argyropoulos,  
797 G., Voutsas, D., Samara, C., and Eleftheriadis, K.: Evolution of air pollution source contributions over one decade,  
798 derived by PM10 and PM2.5 source apportionment in two metropolitan urban areas in Greece, *Atmospheric*  
799 *Environment*, 164, 416–430, <https://doi.org/10.1016/j.atmosenv.2017.06.016>, 2017.
- 800 Dominutti, P. A., Borlaza, L., Sauvain, J. J., Thuy, V. D. N., Houdier, S., Suarez, G., Jaffrezo, J. L., Tobin, S.,  
801 Trébuchon, C., Socquet, S., Moussu, E., Mary, G., and Uzu, G.: Source apportionment of oxidative potential  
802 depends on the choice of the assay: insights into 5 protocols comparison and implications for mitigation measures,  
803 *Environmental Science: Atmospheres*, <https://doi.org/10.1039/d3ea00007a>, 2023.
- 804 Ducret-stich, R. E. and Tsai, M.: RESEARCH ARTICLE PM 10 source apportionment in a Swiss Alpine valley  
805 impacted by highway traffic, 6496–6508, <https://doi.org/10.1007/s11356-013-1682-1>, 2013.
- 806 Espen Yttri, K., Canonaco, F., Eckhardt, S., Evangelidou, N., Fiebig, M., Gundersen, H., Hjellbrekke, A. G., Lund  
807 Myhre, C., Matthew Platt, S., Prevot, A. S. H., Simpson, D., Solberg, S., Surratt, J., Tørseth, K., Uggerud, H.,  
808 Vadset, M., Wan, X., and Aas, W.: Trends, composition, and sources of carbonaceous aerosol at the Birkenes  
809 Observatory, northern Europe, 2001-2018, *Atmospheric Chemistry and Physics*, 21, 7149–7170,  
810 <https://doi.org/10.5194/acp-21-7149-2021>, 2021.
- 811 European committee for standardization: Ambient air - Determination of the concentration of levoglucosan -  
812 Chromatographic method, CEN-CENELEC Management Centre, 2024.



- 813 Fadel, M., Courcot, D., Delmaire, G., Roussel, G., Afif, C., and Ledoux, F.: Source apportionment of PM<sub>2.5</sub>  
814 oxidative potential in an East Mediterranean site, *Science of the Total Environment*, 900,  
815 <https://doi.org/10.1016/j.scitotenv.2023.165843>, 2023.
- 816 Favez, O., El Haddad, I., Piot, C., Boréave, A., Abidi, E., Marchand, N., Jaffrezo, J. L., Besombes, J. L.,  
817 Personnaz, M. B., Sciare, J., Wortham, H., George, C., and D'Anna, B.: Inter-comparison of source apportionment  
818 models for the estimation of wood burning aerosols during wintertime in an Alpine city (Grenoble, France),  
819 *Atmospheric Chemistry and Physics*, 10, 5295–5314, <https://doi.org/10.5194/acp-10-5295-2010>, 2010.
- 820 Favez, O., Weber, S., Petit, J. E., Alleman, L. Y., Albinet, A., Riffault, V., Chazeau, B., Amodeo, T., Salameh,  
821 D., Zhang, Y., Srivastava, D., Samaké, A., Aujay-Plouzeau, R., Papin, A., Bonnaire, N., Boullanger, C., Chatain,  
822 M., Chevrier, F., Detournay, A., Dominik-Sègue, M., Falhun, R., Garbin, C., Gherzi, V., Grignon, G.,  
823 Levigoureux, G., Pontet, S., Rangognio, J., Zhang, S., Besombes, J. L., Conil, S., Uzu, G., Savarino, J., Marchand,  
824 N., Gros, V., Marchand, C., Jaffrezo, J. L., and Leoz-Garziandia, E.: Overview of the French operational network  
825 for in situ observation of PM chemical composition and sources in urban environments (CARA program),  
826 *Atmosphere*, 12, <https://doi.org/10.3390/atmos12020207>, 2021.
- 827 Font, A., Ciupek, K., Butterfield, D., and Fuller, G. W.: Long-term trends in particulate matter from wood burning  
828 in the United Kingdom: Dependence on weather and social factors, *Environmental Pollution*, 314, 120105,  
829 <https://doi.org/10.1016/j.envpol.2022.120105>, 2022.
- 830 Font, A., F. De Brito, J., Riffault, V., Conil, S., Jaffrezo, J.-L., and Bourin, A.: Do rural background sites capture  
831 changes in primary PM<sub>2.5</sub> emissions at the national scale? Recent trends in PM<sub>2.5</sub> and its main components in  
832 metropolitan France., <https://doi.org/10.5194/egusphere-egu25-10935>, 2025.
- 833 Fuzzi, S., Baltensperger, U., Carslaw, K., Decesari, S., Denier Van Der Gon, H., Facchini, M. C., Fowler, D.,  
834 Koren, I., Langford, B., Lohmann, U., Nemitz, E., Pandis, S., Riipinen, I., Rudich, Y., Schaap, M., Slowik, J. G.,  
835 Spracklen, D. V., Vignati, E., Wild, M., Williams, M., and Gilardoni, S.: Particulate matter, air quality and climate:  
836 Lessons learned and future needs, *Atmospheric Chemistry and Physics*, 15, 8217–8299,  
837 <https://doi.org/10.5194/acp-15-8217-2015>, 2015.
- 838 Gama, C., Monteiro, A., Pio, C., Miranda, A. I., Baldasano, J. M., and Tchepel, O.: Temporal patterns and trends  
839 of particulate matter over Portugal: a long-term analysis of background concentrations, *Air Quality, Atmosphere  
840 and Health*, 11, 397–407, <https://doi.org/10.1007/s11869-018-0546-8>, 2018.
- 841 Gary Norris, Rachelle Duvall, Steve Brown, and Song Bai: EPA Positive Matrix Factorization (PMF) 5.0  
842 Fundamentals and User Guide, 2014.
- 843 Gianini, M. F. D., Fischer, A., Gehrig, R., Ulrich, A., Wichser, A., Piot, C., Besombes, J. L., and Hueglin, C.:  
844 Comparative source apportionment of PM<sub>10</sub> in Switzerland for 2008/2009 and 1998/1999 by Positive Matrix  
845 Factorisation, *Atmospheric Environment*, 54, 149–158, <https://doi.org/10.1016/j.atmosenv.2012.02.036>, 2012.
- 846 Glojek, K., Močnik, G., Alas, H. D. C., Cuesta-Mosquera, A., Drinovec, L., Gregorič, A., Ogrin, M., Weinhold,  
847 K., Ježek, I., Müller, T., Rigler, M., Remškar, M., Van Pinxteren, D., Herrmann, H., Ristorini, M., Merkel, M.,  
848 Markelj, M., and Wiedensohler, A.: The impact of temperature inversions on black carbon and particle mass  
849 concentrations in a mountainous area, *Atmospheric Chemistry and Physics*, 22, 5577–5601,  
850 <https://doi.org/10.5194/acp-22-5577-2022>, 2022.
- 851 Glojek, K., Thuy, V. D. N., Weber, S., Uzu, G., Manousakas, M., Elazzouzi, R., Džepina, K., Darfeuil, S., Ginot,  
852 P., Jaffrezo, J. L., Žabkar, R., Turšič, J., Podkoritnik, A., and Močnik, G.: Annual variation of source contributions  
853 to PM<sub>10</sub> and oxidative potential in a mountainous area with traffic, biomass burning, cement-plant and biogenic  
854 influences, *Environment International*, 189, 108787, <https://doi.org/10.1016/j.envint.2024.108787>, 2024.
- 855 Goldfeld, S. M. and Quandt, R. E.: Some Tests for Homoscedasticity Author (s): Stephen M. Goldfeld and  
856 Richard E. Quandt Source: *Journal of the American Statistical Association*, Jun., 1965, Vol. 60, No. 310  
857 Published by: Taylor & Francis, Ltd. on behalf of the American Statistical Association, *Journal of the American Statistical  
858 Association*, 60, 539–547, 1965.
- 859 Grantz, D. A., Garner, J. H. B., and Johnson, D. W.: Ecological effects of particulate matter, *Environment  
860 International*, 29, 213–239, [https://doi.org/10.1016/S0160-4120\(02\)00181-2](https://doi.org/10.1016/S0160-4120(02)00181-2), 2003.



- 861 Hopke, P. K.: Review of receptor modeling methods for source apportionment, *Journal of the Air and Waste*  
862 *Management Association*, 66, 237–259, <https://doi.org/10.1080/10962247.2016.1140693>, 2016.
- 863 Hopke, P. K., Dai, Q., Li, L., and Feng, Y.: Global review of recent source apportionments for airborne particulate  
864 matter, *Science of The Total Environment*, 740, 140091, <https://doi.org/10.1016/j.scitotenv.2020.140091>, 2020.
- 865 Largeron, Y. and Staquet, C.: Persistent inversion dynamics and wintertime PM<sub>10</sub> air pollution in Alpine valleys,  
866 *Atmospheric Environment*, 135, 92–108, <https://doi.org/10.1016/j.atmosenv.2016.03.045>, 2016.
- 867 Li, Xia, T., and Nel, A. E.: The role of oxidative stress in ambient particulate matter-induced lung diseases and its  
868 implications in the toxicity of engineered nanoparticles, *Free Radical Biology and Medicine*, 44, 1689–1699,  
869 <https://doi.org/10.1016/j.freeradbiomed.2008.01.028>, 2008.
- 870 Li, J., Chen, B., de la Campa, A. M. S., Alastuey, A., Querol, X., and de la Rosa, J. D.: 2005–2014 trends of PM<sub>10</sub>  
871 source contributions in an industrialized area of southern Spain, *Environmental Pollution*, 236, 570–579,  
872 <https://doi.org/10.1016/j.envpol.2018.01.101>, 2018.
- 873 Lodovici, M. and Bigagli, E.: Oxidative stress and air pollution exposure, *Journal of Toxicology*, 2011,  
874 <https://doi.org/10.1155/2011/487074>, 2011.
- 875 Mudway, I. S., Kelly, F. J., and Holgate, S. T.: Oxidative stress in air pollution research, *Free Radical Biology*  
876 *and Medicine*, 151, 2–6, <https://doi.org/10.1016/j.freeradbiomed.2020.04.031>, 2020.
- 877 Nelin, T. D., Joseph, A. M., Gorr, M. W., and Wold, L. E.: Direct and indirect effects of particulate matter on the  
878 cardiovascular system, *Toxicology Letters*, 208, 293–299, <https://doi.org/10.1016/j.toxlet.2011.11.008>, 2012.
- 879 Ngoc Thuy, V. D., Jaffrezou, J.-L., Hough, I., Dominutti, P. A., Salque Moreton, G., Gille, G., Francony, F., Patron-  
880 Anquez, A., Favez, O., and Uzu, G.: Unveiling the optimal regression model for source apportionment of the  
881 oxidative potential of PM<sub>10</sub>, *Atmospheric Chemistry and Physics*, 24, 7261–7282, [https://doi.org/10.5194/acp-24-](https://doi.org/10.5194/acp-24-7261-2024)  
882 7261-2024, 2024.
- 883 O'Brien, R. M.: A caution regarding rules of thumb for variance inflation factors, *Quality and Quantity*, 41, 673–  
884 690, <https://doi.org/10.1007/s11135-006-9018-6>, 2007.
- 885 Paatero, P. and Tappert, U.: Positive matrix factorization: A non-negative factor model with optimal utilization  
886 of error estimates of data values, *Environmetrics*, <https://doi.org/10.1002/env.3170050203>, 1994.
- 887 Pandolfi, M., Alastuey, A., Pérez, N., Reche, C., Castro, I., Shatalov, V., and Querol, X.: Trends analysis of PM  
888 source contributions and chemical tracers in NE Spain during 2004–2014: A multi-exponential approach,  
889 *Atmospheric Chemistry and Physics*, 16, 11787–11805, <https://doi.org/10.5194/acp-16-11787-2016>, 2016.
- 890 Pietrodangelo, A., Bove, M. C., Forello, A. C., Crova, F., Bigi, A., Brattich, E., Riccio, A., Becagli, S., Bertinetti,  
891 S., Calzolari, G., Canepari, S., Cappelletti, D., Catrambone, M., Cesari, D., Colombi, C., Contini, D., Cuccia, E.,  
892 De Gennaro, G., Genga, A., Ielpo, P., Lucarelli, F., Malandrino, M., Masiol, M., Massabò, D., Perrino, C., Prati,  
893 P., Siciliano, T., Tositti, L., Venturini, E., and Vecchi, R.: A PM<sub>10</sub> chemically characterized nation-wide dataset  
894 for Italy. Geographical influence on urban air pollution and source apportionment, *Science of The Total*  
895 *Environment*, 908, 167891, <https://doi.org/10.1016/j.scitotenv.2023.167891>, 2024.
- 896 Pietrogrande, M. C., Romanato, L., and Russo, M.: Synergistic and Antagonistic Effects of Aerosol Components  
897 on Its Oxidative Potential as Predictor of Particle Toxicity, *Toxics*, 10, <https://doi.org/10.3390/toxics10040196>,  
898 2022.
- 899 Pope, C. A. and Dockery, D. W.: Health effects of fine particulate air pollution: Lines that connect, *Journal of the*  
900 *Air and Waste Management Association*, 56, 709–742, <https://doi.org/10.1080/10473289.2006.10464485>, 2006.
- 901 Rao, X., Zhong, J., Brook, R. D., and Rajagopalan, S.: Effect of Particulate Matter Air Pollution on Cardiovascular  
902 Oxidative Stress Pathways, Antioxidants and Redox Signaling, 28, 797–818,  
903 <https://doi.org/10.1089/ars.2017.7394>, 2018.



- 904 Robert B Cleveland, William S. Cleveland, Jean E. McRae, and Irma Terpenning: STL: A Seasonal-Trend  
905 decomposition Procedure Based on Loess, 1990.
- 906 Rosenblad, A.: The Concise Encyclopedia of Statistics, 867–868 pp.,  
907 <https://doi.org/10.1080/02664760903075614>, 2011.
- 908 Samake, A., Uzu, G., Martins, J. M. F., Calas, A., Vince, E., Parat, S., and Jaffrezo, J. L.: The unexpected role of  
909 bioaerosols in the Oxidative Potential of PM, Scientific Reports, 7, <https://doi.org/10.1038/s41598-017-11178-0>,  
910 2017.
- 911 Samaké, A., Jaffrezo, J. L., Favez, O., Weber, S., Jacob, V., Canete, T., Albinet, A., Charron, A., Riffault, V.,  
912 Perdrix, E., Waked, A., Golly, B., Salameh, D., Chevrier, F., Miguel Oliveira, D., Besombes, J. L., Martins, J. M.  
913 F., Bonnaire, N., Conil, S., Guillaud, G., Mesbah, B., Rocq, B., Robic, P. Y., Hulin, A., Le Meur, S.,  
914 Descheemaeker, M., Chretien, E., Marchand, N., and Uzu, G.: Arabitol, mannitol, and glucose as tracers of  
915 primary biogenic organic aerosol: The influence of environmental factors on ambient air concentrations and  
916 spatial distribution over France, Atmospheric Chemistry and Physics, 19, 11013–11030,  
917 <https://doi.org/10.5194/acp-19-11013-2019>, 2019a.
- 918 Samaké, A., Jaffrezo, J. L., Favez, O., Weber, S., Jacob, V., Albinet, A., Riffault, V., Perdrix, E., Waked, A.,  
919 Golly, B., Salameh, D., Chevrier, F., Miguel Oliveira, D., Bonnaire, N., Besombes, J. L., Martins, J. M. F., Conil,  
920 S., Guillaud, G., Mesbah, B., Rocq, B., Robic, P. Y., Hulin, A., Le Meur, S., Descheemaeker, M., Chretien, E.,  
921 Marchand, N., and Uzu, G.: Polyols and glucose particulate species as tracers of primary biogenic organic aerosols  
922 at 28 French sites, Atmospheric Chemistry and Physics, 19, 3357–3374, [https://doi.org/10.5194/acp-19-3357-](https://doi.org/10.5194/acp-19-3357-2019)  
923 2019, 2019b.
- 924 Seabold, S. and Perktold, J.: Statsmodels: Econometric and statistical modeling with python, in: 9th Python in  
925 Science Conference, 2010.
- 926 Srivastava, D., Tomaz, S., Favez, O., Lanzafame, G. M., Golly, B., Besombes, J. L., Alleman, L. Y., Jaffrezo, J.  
927 L., Jacob, V., Perraudin, E., Villenave, E., and Albinet, A.: Speciation of organic fraction does matter for source  
928 apportionment. Part 1: A one-year campaign in Grenoble (France), Science of the Total Environment, 624, 1598–  
929 1611, <https://doi.org/10.1016/j.scitotenv.2017.12.135>, 2018.
- 930 Tomaz, S., Shahpoury, P., Jaffrezo, J. L., Lammel, G., Perraudin, E., Villenave, E., and Albinet, A.: One-year  
931 study of polycyclic aromatic compounds at an urban site in Grenoble (France): Seasonal variations, gas/particle  
932 partitioning and cancer risk estimation, Science of the Total Environment, 565, 1071–1083,  
933 <https://doi.org/10.1016/j.scitotenv.2016.05.137>, 2016.
- 934 Tomaz, S., Jaffrezo, J. L., Favez, O., Perraudin, E., Villenave, E., and Albinet, A.: Sources and atmospheric  
935 chemistry of oxy- and nitro-PAHs in the ambient air of Grenoble (France), Atmospheric Environment, 161, 144–  
936 154, <https://doi.org/10.1016/j.atmosenv.2017.04.042>, 2017.
- 937 Veld, M. in 't, Pandolfi, M., Amato, F., Pérez, N., Reche, C., Dominutti, P., Jaffrezo, J., Alastuey, A., Querol, X.,  
938 and Uzu, G.: Discovering oxidative potential (OP) drivers of atmospheric PM<sub>10</sub>, PM<sub>2.5</sub>, and PM<sub>1</sub> simultaneously  
939 in North-Eastern Spain, Science of the Total Environment, 857, <https://doi.org/10.1016/j.scitotenv.2022.159386>,  
940 2023.
- 941 Via, M., Yus-Díez, J., Canonaco, F., Petit, J. E., Hopke, P., Reche, C., Pandolfi, M., Ivančić, M., Rigler, M.,  
942 Prevôt, A. S. H., Querol, X., Alastuey, A., and Minguillón, M. C.: Towards a better understanding of fine PM  
943 sources: Online and offline datasets combination in a single PMF, Environment International, 177,  
944 <https://doi.org/10.1016/j.envint.2023.108006>, 2023.
- 945 Viana, M., Kuhlbusch, T. A. J., Querol, X., Alastuey, A., Harrison, R. M., Hopke, P. K., Winiwarter, W., Vallius,  
946 M., Szidat, S., Prevôt, A. S. H., Hueglin, C., Bloemen, H., Wählin, P., Vecchi, R., Miranda, A. I., Kasper-Giebl,  
947 A., Maenhaut, W., and Hitznerberger, R.: Source apportionment of particulate matter in Europe: A review of  
948 methods and results, <https://doi.org/10.1016/j.jaerosci.2008.05.007>, 2008.
- 949 Vida, M., Foret, G., Siour, G., Coman, A., Weber, S., Favez, O., Jaffrezo, J. L., Pontet, S., Mesbah, B., Gille, G.,  
950 Zhang, S., Chevrier, F., Pallares, C., Uzu, G., and Beekmann, M.: Oxidative potential modelling of PM<sub>10</sub>: a 2-  
951 year study over France, ACDP, 2024.



- 952 Waked, A., Favez, O., Alleman, L. Y., Piot, C., Petit, J. E., Delaunay, T., Verlinden, E., Golly, B., Besombes, J.  
953 L., Jaffrezo, J. L., and Leoz-Garziandia, E.: Source apportionment of PM<sub>10</sub> in a north-western Europe regional  
954 urban background site (Lens, France) using positive matrix factorization and including primary biogenic  
955 emissions, *Atmospheric Chemistry and Physics*, 14, 3325–3346, <https://doi.org/10.5194/acp-14-3325-2014>, 2014.
- 956 Weber, S., Uzu, G., Calas, A., Chevrier, F., Besombes, J. L., Charron, A., Salameh, D., Ježek, I., Močnik, G., and  
957 Jaffrezo, J. L.: An apportionment method for the oxidative potential of atmospheric particulate matter sources:  
958 Application to a one-year study in Chamonix, France, *Atmospheric Chemistry and Physics*, 18, 9617–9629,  
959 <https://doi.org/10.5194/acp-18-9617-2018>, 2018.
- 960 Weber, S., Salameh, D., Albinet, A., Alleman, L. Y., Waked, A., Besombes, J.-L., Jacob, V., Guillaud, G.,  
961 Meshbah, B., Rocq, B., Hulin, A., Dominik-Sègue, M., Chrétien, E., Jaffrezo, J.-L., and Favez, O.: Comparison  
962 of PM<sub>10</sub> Sources Profiles at 15 French Sites Using a Harmonized Constrained Positive Matrix Factorization  
963 Approach, *Atmosphere*, 10, 310, <https://doi.org/10.3390/atmos10060310>, 2019.
- 964 Weber, S., Uzu, G., Favez, O., Borlaza, L., Calas, A., Salameh, D., Chevrier, F., Allard, J., Besombes, J. L.,  
965 Albinet, A., Pontet, S., Mesbah, B., Gille, G., Zhang, S., Pallares, C., Leoz-Garziandia, E., and Jaffrezo, J. L.:  
966 Source apportionment of atmospheric PM<sub>10</sub> oxidative potential: Synthesis of 15 year-round urban datasets in  
967 France, *Atmospheric Chemistry and Physics*, 21, 11353–11378, <https://doi.org/10.5194/acp-21-11353-2021>,  
968 2021.
- 969 Xiong, Q., Yu, H., Wang, R., Wei, J., and Verma, V.: Rethinking Dithiothreitol-Based Particulate Matter  
970 Oxidative Potential: Measuring Dithiothreitol Consumption versus Reactive Oxygen Species Generation,  
971 *Environmental Science and Technology*, 51, 6507–6514, <https://doi.org/10.1021/acs.est.7b01272>, 2017.

972